nature portfolio

https://doi.org/10.1038/s41586-024-08396-8

Supplementary information

Methane emissions from the Nord Stream subsea pipeline leaks

In the format provided by the authors and unedited

Supplementary Information

Methane emissions from the Nord Stream subsea pipeline leaks

Supplementary Table 1 | Summary of bottom-up (BU) and top-down (TD) approaches used to estimate the various components of CH_4 emissions from the Nord Stream pipeline leaks.

Method[a]	Estimate[b]	Description	Limitations & Comments
			Bottom-up
Pipeline estimates[c]			
Volumetric calculation Ref. 1 Published: 28/09/22	300 kt	Volumetric calculation of CH_4 released from all ruptured pipelines.	*Limitations* • Calculations performed using parameters only for NS2A (100 kt) and multiplied by three. Does not reliably estimate the volume of CH_4 released from the three ruptured pipelines. • Assumptions made for pipeline initial and final pressure (100 and 7 bar), gas temperature (10°C), natural gas composition (100% CH_4), pipeline lengths (1250 km) and inner diameter (1100 mm). Several of these values are inconsistent with those derived in the present study (Extended Data Tables 1,2). *Comments* • Rapidly disseminated the broad magnitude of pipeline CH_4 emissions to global community.
Volumetric calculation Ref. 110 Published: 28/09/22	100–400 kt	Volumetric calculation of CH_4 contained within all pipelines prior to rupturing.	*Limitations* • Parameters used in the estimations are not reported. *Comments* • Estimations based on natural gas volumes in the three pipelines prior to rupturing reported by ref. 5 (778 million standard cubic meters (MSm^3) natural gas). • Ambiguous with regards to which volumetric estimates correspond to which pipeline, and the total amount contained across the three ruptured pipelines. • Rapidly disseminated the broad magnitude of potential pipeline CH_4 emissions to global community.
Volumetric calculation Ref. 3 Published: 10/10/23	509 kt	Volumetric calculation of CH_4 contained within all pipelines prior to rupturing.	*Comments* • Estimations based on natural gas volumes in the three pipelines prior to rupturing reported by ref. 5 (778 MSm^3 natural gas)[d]. • Estimates the effect of the northernmost leak site on NS2A pipeline emission rates (Supplementary Discussion 1).
Volumetric calculation Ref. 4 Published: 30/09/22	352 kt	Volumetric calculation of CH_4 contained within all pipelines prior to rupturing.	*Limitations* • Assumes 500 MSm^3 of CH_4 was contained within the three pipelines. This is inconsistent with volumes reported by ref. 5 based on information provided by pipeline operators. Does not reliably estimate the volume of CH_4 released from the three ruptured pipelines. *Comments* • Rapidly disseminated the broad magnitude of potential pipeline CH_4 emissions to global community. • Relates the estimate to total global, global ocean, Baltic Sea, and permafrost CH_4 emissions to the atmosphere and addresses expected risks for the marine environment.
Volumetric calculation	501 kt[d]	Volumetric calculation of	*Comments*

Method[a]	Estimate[b]	Description	Limitations & Comments
Ref. 5 Published: 29/09/22		CH_4 based on natural gas contained within all pipelines prior to rupturing.	• Estimate corresponds to our calculation of CH_4 contained within the three pipelines using the natural gas volumes (778 Msm^3) reported by ref. 5. • Assumes the natural gas contains 93% CH_4 by mass and has a CH_4 density of 0.693 kg/m^3 at 20°C and 1 atmosphere. • Volumes reported by ref. 5 were provided by the pipeline operators.
Volumetric calculation Ref. 8 Published: 26/10/22	230 kt	Volumetric calculation of CH_4 released from all ruptured pipelines.	*Limitations* • Calculations performed using volumetric calculations for NS2A (115 kt) and multiplied by two. Does not reliably estimate the volume of CH_4 released from the three ruptured pipelines. • Assumptions made for initial and final pressure (105 and 7 bar), gas temperature (5°C), natural gas composition (96.5% CH_4), pipeline lengths (1224 km), inner diameter (1153 mm). Several of these values are inconsistent with those derived in the present study (Extended Data Tables 1,2). • Comparisons made to TD estimates do not account for marine dissolution, oxidation, and sea-surface outgassing. *Comments* • First comparison to TD tall tower inversion and satellite estimates in the literature.
Volumetric calculation Ref. 2 Published: 30/09/22	115 kt	Volumetric calculation of CH_4 contained within the NS2A pipeline prior to rupturing.	*Limitations* • Parameters used in the estimation are not reported. *Comments* • Rapidly disseminated the broad magnitude of potential pipeline CH_4 emissions from NS2A to global community.
Volumetric calculation Ref. 111 Published: 29/09/22	100 kt	Volumetric calculation of CH_4 contained within the NS2A pipeline prior to rupturing.	*Limitations* • Parameters used in the estimation are not reported. *Comments* • Article estimates that NS2 pipelines (NS2A and NS2B) contained 300 MSm^3 natural gas equivalent to 200 kt CH_4. Accordingly, we have inferred that 100 kt CH_4 was estimated for NS2A. • Rapidly disseminated the broad magnitude of potential pipeline CH_4 emissions from NS2A to global community.
Volumetric calculation Ref. 112 Published: 29/09/22	90-135 kt	Volumetric calculation of CH_4 released from the NS2A after rupturing.	*Limitations* • Parameters used in the estimation are not reported. *Comments* • Article estimates that NS2 pipelines (NS2A and NS2B) contained 180-270 kt CH_4. Accordingly, we have inferred that 90-135 kt CH_4 was estimated for NS2A. • Rapidly disseminated the broad magnitude of potential pipeline CH_4 emissions from NS2A to global community.
Volumetric calculation *This study*	496±14 kt	Volumetric calculation of CH_4 contained within all ruptured pipelines prior to rupturing.	*Comments* • Derived using parameters outlined in Extended Data Table 1 and 2, including their uncertainty. • Volumetric estimates are consistent with initial pipeline inventories reported by pipeline operators to ref. 5[d].

Method[a]	Estimate[b]	Description	Limitations & Comments
Pipeline emission simulation Ref. 6 Published: 19/04/24	330 kt	Time series simulations of CH_4 released from all ruptured pipelines using idealized physical concepts, and simulation of atmospheric plumes using SILAM[113].	*Limitations* • Assumes the initial pressure is 105 bar in all three pipelines. This is inconsistent with those derived in the present study (Extended Data Tables 1,2). Does not reliably estimate the volume of CH_4 released from the three ruptured pipelines. • No uncertainty analysis (both in the model and input) is provided. • Does not consider the effect of the second northernmost partial rupture on NS2A emission rates. • No energy conservation equation is considered: a constant gas temperature is assumed during the gas release despite our CATHARE simulations showing gas temperature reached as low as -85°C. • No advection term is used in the momentum conservation equation. • Uses a simplified EOS, which can lead to discrepancies in the cumulative mass of CH_4 computed by the model. These discrepancies are not evaluated. *Comments* • Verifies the relative timing (not magnitude) of the modelled time series of emission rates by qualitatively comparing them with TD ICOS tall tower observations, and observations from monitoring stations in Estonia and Finland. • Considers the initial height of plume release using an existing parametrization for wild-fire plume injection height.
Pipeline emission simulation Ref. 7 Published: 20/12/23	478 kt	Time series simulations of CH_4 released from all ruptured pipelines using OLGA[114].	*Limitations* • Contrary to the author's statements, the estimate does not equate to atmospheric CH_4 emissions because marine dissolution, oxidation, and sea-surface outgassing are not quantified. • No uncertainty analysis (both in the model and output) is provided. • Assumes the initial pressure is 175 bar in NS1 pipelines. A reference for this initial pressure is not provided and is inconsistent with those derived in the present study (Extended Data Tables 1,2). • No emission rate time series are reported; TD point-in-time emission rates estimates cannot be compared to verify the modelled pipeline emissions. • Software package driven by user; model uncertainty is not tested or quantified. • Does not consider the effect of the second northernmost partial rupture on NS2A emission rates. *Comments* • Provides time series of aggregated pipeline CH_4 emissions from the three ruptured pipelines.
Pipeline emission rate simulation *This study*	457±14 kt	Time series simulations of CH_4 released from all ruptured pipelines using PBREAK[36].	*Limitations* • Uses a simplified EOS, leading to a mass discrepancy of 3% in the modelled cumulative CH_4 released from the pipelines compared to initial pipeline inventories (see Extended Data Table 3). • Software package driven by user; model uncertainty is not tested or quantified.

Method[a]	Estimate[b]	Description	Limitations & Comments
			• Does not consider the effect of the second northernmost partial rupture on NS2A emission rates. *Comments* • Considers uncertainty in pipeline characteristics (Extended Data Tables 1 and 2). • Model previously used to model pipeline emission rates from pipeline ruptures[48,49].
Pipeline emission rate simulation *This study*	472±14 kt	Time series simulations of CH_4 released from all ruptured pipelines using CATHARE[37].	*Limitations* • Does not consider the effect of the second northernmost partial rupture on NS2A emission rates. *Comments* • Provides a time series of pipeline emission rates, gas pressure, temperature, gas velocities, landfall pressure, and Froude constants from each pipeline. • Tests performed to validate the code's suitability to model single phase pipeline ruptures (Supplementary Method 1). • Considers uncertainty in pipeline characteristics (Extended Data Tables 1,2) and model sensitivities. Code is customisable by the user. • Model uses natural gas EOS (see Supplementary Discussion 3). Provides an accurate estimate of cumulative pipeline emissions with low mass discrepancy (0.3%) in the modelled cumulative CH_4 released from the pipelines compared to initial pipeline inventories (see Extended Data Table 3). • Emission rate velocities at the break site from each pipeline are used in Inversion 6 to estimate the vertical dispersion of the plume.
Marine estimate[e]			
Marine bubble plume modelling Ref. 39 Published: 07/09/23	Dissolved: 11 kt Outgassed: 8 kt Oxidised: 3 kt	Near-field bubble plume simulations using the Texas A&M oil spill calculator (TAMOC)[115] coupled to a Lagrangian far-field chemical transport model.	*Limitations* • Simulations assume 215 kt CH_4 released from pipelines, contrary to PBREAK and CATHARE estimates (see Extended Data Table 3). • Oxidation estimate derived using maximum oxidation rates at a site in the North Sea where high CH_4 concentrations were present for nearly 30 years without interruption. • Estimates do not incorporate TD measurements. Thus, estimates have not been calibrated/verified through direct measurement (c.f., refs. 9,10). *Comments* • Only assessment of CH_4 oxidation in the literature. • First estimates of magnitude of marine dissolution and outgassing in the literature. • Spatially resolves CH_4 dissolved in, and outgassed from, the Baltic Sea. • Despite using a different amount of CH_4 from the pipelines to the present study, estimates for CH_4 dissolution and outgassing are consistent with top-down approaches[9,10]. • The TAMOC model was previously used to model the Deepwater Horizon disaster[116].
		Top-down	
Marine and ship-based estimates[e]			
Glider, SOOP, and plume modelling	Dissolved: 9–15 kt. Outgassed: 8–13 kt.	Regional modelling of CH_4 dissolution and outgassing	*Limitations* • First autonomous glider measurements were obtained after the leaks had stopped.

Method[a]	Estimate[b]	Description	Limitations & Comments
Ref. 9 Published: 10/2024	Outgassing rates: 0–74 t/hr. Data acquired: 05/10/22 to 01/01/23 (ocean glider) and 26/09/22 to 01/01/23 (SOOP).	based on PBREAK and CATHARE pipeline emission rates (*this study*), calibrated using autonomous glider and SOOP measurements.	• Significant spatial uncertainty in the accumulation of dissolved CH_4 over long periods due to possible inaccuracies in ocean current transport modelling. • Average natural background CH_4 concentrations (10nM) were assumed due to lack of measurements prior to leaks. • Limited spatial coverage of observations. *Comments* • SOOP measurements available from onset of leaks. • Glider and SOOP approaches acquire continuous data, providing improved temporal coverage compared to discrete sampling approaches. • Gliders provide observations of dissolved CH_4 in high vertical and horizontal resolution close to the leak sites. SOOP observations improves spatial coverage in the surface layer. • Direct link to PBREAK and CATHARE pipeline emission models allows for computation of NAER and NAE for comparison to other TD estimates. • Uncertainty in PBREAK and CATHARE pipeline emission rates are propagated into the dissolution and outgassing estimates.
CTD casts and plume modelling Ref. 10 Published: 19/06/24	Dissolved: 10 kt[f]. Data acquired: 03/10/22 to 05/10/22.	Regional modelling of CH_4 dissolution based on discrete CTD sampling.	*Limitations* • First CTD measurements were obtained after leaks had stopped. • Discrete sampling only provides snapshot of dissolved CH_4 over a three-day period with limited lateral resolution and coverage. • Uncertainty related to modelling ocean currents over the period of weeks is not quantified. • Subsea plume simulations quantify dissolved CH_4; no CH_4 outgassing is modelled. *Comments* • An upper estimate of 55 kt is reported, which is derived from a maximum CH_4 concentration measured from a single sample site. We assess that the lower reported estimate of 10 kt, which is derived from average CH_4 concentrations measured across 16 sites, is a more reliable estimate of the total amount of dissolved CH_4. • Isotopic measurements allow for clearer distinction of fossil gas sources from natural background dissolved CH_4 concentrations. • Provides good vertical resolution of the structure of the dissolved CH_4 plumes at sampling locations. • Modelling is independent of the PBREAK and CATHARE emission rates reported in the present study.
Air sampling onboard RV Skagerrak Ref. 10 Published: 19/06/24	Outgassing rates: $0.5–5\times10^{-3}$ t/hr/km^2. Data acquired: 03/10/22 17:50 to 04/10/22 03:55, 04/10/22 20:10 to	Estimation of atmospheric CH_4 emissions from sea-surface outgassing using sea-air gas exchange calculations.	*Limitations* • Sampling mostly restricted to night-time, which may have enhanced atmospheric concentrations due to lowering of the nocturnal boundary layer. • Sampling restricted to CTD sampling sites limited to the northernmost leak sites. • No sub-regional modelling conducted to upscale outgassing rates to the wider spatial extent previously estimated to have undergone outgassing (see refs. 9,11). *Comments* • Further confirmation of the occurrence of sea-surface outgassing in vicinity of the northern leak sites as

Method[a]	Estimate[b]	Description	Limitations & Comments
	05/10/22 04:00, and 05/10/22 17:30 to 06/10/22 13:00.		quantified using HELiPOD[11], and as modelled using glider and SOOP observations[9].
Airborne estimates[g]			
HELiPOD Ref. 11 Published: 10/2024	Outgassing rates: 19–48 t/hr. Data acquired: 05/10/22 08:00 to 15:30.	Sub-regional modelling of atmospheric CH_4 emissions from sea-surface outgassing using HELiPOD[41].	*Limitations* • Time needed to coordinate measurement campaign (e.g., availability of instrument, personnel, and flight permits) prevented quantifying the initial emissions from bubbles transported to the surface. • Measurement time is limited by flight duration. • Flight exclusion zones reduced the spatial coverage of the flights. *Comments* • Provided on-site verification of sea-surface outgassing rates and outgassed emissions after leaking had stopped, which were not detectable using satellites or ICOS tall tower stations. • Only in-situ measurement and modelling of atmospheric CH_4 concentrations above all leak sites (c.f. ship-based approach in ref. 10).
Satellite estimates[g]			
S-2B Ref. 8 Published: 26/10/22	72±38 t/hr Data acquired: 30/09/22 10:07.	IME method[42] applied to S-2B nadir observations over the NS2A leak site.	*Limitations* • Cloud cover prevented quantification in days prior. • Spectral reflectance of bubbles may have contributed substantially to the observed radiance. • S-2B imagery over the leak site likely missed large parts of the plume that extended over water because water absorbs sunlight in the Shortwave Infrared (SWIR) range. *Comments* • S-2B satellite is typically poorly sensitive over water. Detection of Nord Stream plumes only possible due to the bright patch of sea foam which created sufficient spectral reflectance.
L8 and S-2B ensemble Ref. 12 Published: 08/05/24	502±464 t/hr Data acquired: 29/09/22 09:56 (L8) and 30/09/22 10:15 (S-2B).	Ensemble approach applying MBSP and IME methods[42,43] to L8 and S-2B nadir observations over the NS2A leak site.	*Limitations* • Cloud cover prevented quantification in days prior. *Comments* • L8 and S-2B satellites are typically poorly sensitive over water. Detection of Nord Stream plumes only possible due to the bright patch of sea foam which created sufficient spectral reflectance. • Incorporates an empirical calibration of sea-foam albedo spectral dependence using sea-foam observations in ship trails. • Incorporates a tailored effective wind speed calibration that accounts for the partial plume observation (i.e., the plume was only detected over the bright sea foam patch). • Reported expanded uncertainty likely better reflects the limitations of offshore point-source quantification using L8 and S-2B.
GHGSat Ref. 13 Published: 01/02/24	C2: not quantified (30/09/22 08:51).	GHGSat quantifications over the southern NS2A leak	*Limitations* • 1-day lead time needed for tasking. • Cloud cover prevented quantification in days prior.

Method[a]	Estimate[b]	Description	Limitations & Comments
	C1: 84±24 t/hr (30/09/22 10:27). C4: 24±8 t/hr (30/09/22 12:54).	site using a glint observation mode.	• Quantifications dependent on scattering angle and reflectivity for offshore detections; 2 out of 3 detections over the NS2A leak site were quantifiable. *Comments* • GHGSat constellation can achieve high cross track and along track angles, which enables more opportunities for glint observations and quantifications over water (c.f., S-2B and L8 nadir observations in refs. 8,12). • Low detection limits for offshore detections of between 160-600 kg/hr CH_4.
IASI - Inversion Ref. 14 Published: 24/09/2024	219–427 kt Atmospheric emissions quantified to: 28/09/22 00:00.	Regional inverse modelling of atmospheric CH_4 emissions using IASI observations coupled to the TOMCAT[60] transport model.	*Limitations* • Transport model operated at coarse 1° × 1° horizontal resolution, unlikely to resolve the fine-scale transport of the three plumes. • Uncertainties are introduced due to the instantaneous mixing of the leak emissions horizontally across model grid boxes. • Biases in the model transport parameterisations, particularly for vertical mixing, can lead to incorrect simulated vertical distribution of the plume. • Uses assumed exponential prior emission rates. *Comments* • IASI is typically poorly sensitive to lower atmospheric layers, therefore not always suited to surficial CH_4 research. • IASI measures the spectrum of infrared radiation over the Earth's surface rather than reflectance, allowing offshore detection not reliant on sunlight (c.f. L8, S-2B and the GHGSat constellation).
IASI - IME Method Ref. 14 Published: 24/09/2024	30±1 kt (26/09/22 07:30) 16±1 kt (27/09/22 19:30) 161±4 kt (28/09/22 07:30) 77±2 kt (28/09/22 19:30)	IASI XCH_4 data modelled using the IME method[42].	*Limitations* • IME method as applied does not take account of IASI's vertical sensitivity, which is highest in the upper troposphere, introducing a negative bias to the results. • Possible that not all the CH_4 emitted from the leak was viewed by the satellite due to cloud coverage, introducing a further negative bias to results. *Comments* • Boundaries for CH_4 enhancements constrained using Hybrid Single Particle Lagrangian Integrated Trajectory (HYSPLIT) trajectory analysis.
IASI - Inversion 1 *This study*	281–346 kt Atmospheric emissions quantified to: 28/09/22 00:00.	Regional inverse modelling of atmospheric CH_4 emissions using IASI observations coupled to the TOMCAT[60] transport model.	*Limitations* • As in ref. 14 (see above). *Comments* • Revision of the ref. 14 estimate (see above). • Incorporates updated emission priors (P-NAER and C-NAER) from each leak site, including their temporal error covariances. • The reported range accounts for differences in emission rate priors (P-NAER and C-NAER) and whether the inversions are optimised against individual or mean IASI column retrievals. • Estimate has reduced uncertainty compared to ref. 14.

Method[a]	Estimate[b]	Description	Limitations & Comments
Tall tower estimates[g]			
Inversion Ref. 8 Published: 26/10/22	220±30 kt Atmospheric emissions quantified to: 01/10/22 11:00.	Tall tower inversion modelled using WRF-CMAQ (M1 in ref. 8) to derive total atmospheric CH_4 emissions.	*Limitations* • Plumes are sparsely detected by the tall towers. Modelling is heavily dependent on the temporal profiles of the initial assumed emission rate. • Uses NRT ICOS tall tower data, which had filtered out high CH_4 mixing ratios at some ICOS stations, potentially leading to underfitting of emissions. *Comments* • ICOS stations used: BIR, NOR, HTM and UTO.
Inversion Ref. 8 Published: 26/10/22	226±90 kt Atmospheric emissions quantified to: 30/09/22 00:00.	Tall tower inversion modelled using STILT[73,74] (M2 in ref. 8) to derive total atmospheric CH_4 emissions.	*Limitations* • Plumes are sparsely detected by the tall towers. Modelling is heavily dependent on the temporal profiles of the prior. • Uses assumed constant prior emission rates. • Uses NRT ICOS tall tower data, which had filtered out high CH_4 mixing ratios at some ICOS stations, potentially leading to underfitting of emissions. • Effect of buoyancy on plume height at the point of release not considered[h]. *Comments* • ICOS stations used: BIR, NOR, HTM and UTO.
Inversion Ref. 15 Published: 17/10/22	175 kt Atmospheric emissions quantified to: 28/09/22 00:00.	Tall tower inversion using the Integrated Forecasting System (IFS) model to derive total atmospheric CH_4 emissions.	*Limitations* • Plumes are sparsely detected by the tall towers. Modelling is heavily dependent on the temporal profiles of the prior. • Uses assumed constant prior emission rates. • Uses NRT ICOS tall tower data, which had filtered out high CH_4 mixing ratios at some ICOS stations, potentially leading to underfitting of emissions. *Comments* • ICOS stations used: BIR, NOR and HTM. • Full methodology not published.
Inversion Ref. 16 Published: 05/10/22	70 kt Atmospheric emissions quantified to: 03/10/22 23:00.	Tall tower inversion modelled using CHIMERE[82] to derive total atmospheric CH_4 emissions.	*Limitations* • Plumes are sparsely detected by the tall towers. Modelling is heavily dependent on the temporal profiles of the prior. • Uses assumed constant prior emission rates. • Uses NRT ICOS tall tower data, which had filtered out high CH_4 mixing ratios at some ICOS stations, potentially leading to underfitting of emissions. *Comments* • ICOS stations used: BIR and NOR. • Full methodology not published.
Inversion Ref. 17 Published: 01/11/22	90-300 kt Atmospheric emissions quantified to: 03/10/22 23:00.	Tall tower inversion modelled using CHIMERE[82] to derive total atmospheric CH_4 emissions.	*Limitations* • As in ref. 16 (see above). • Uses assumed exponential prior emission rates. *Comments* • ICOS stations used: BIR and NOR. • Revision of the ref. 17 estimate. • Simulations undertaken at fine resolution (0.2°). • Accounts plume buoyancy by simulating vertical profiles of emissions at coarse resolution (every ~200m).
Inversion Ref. 18 Published: 12/10/22	56–155 kt Atmospheric emissions quantified	Tall tower inversion modelled using FLEXPART[65]	*Limitations* • Plumes are sparsely detected by the observations site. Modelling is heavily dependent on the temporal profiles of the prior.

Method[a]	Estimate[b]	Description	Limitations & Comments
	to: 28/09/22 00:00.	to derive total atmospheric CH_4 emissions.	• Uses assumed exponential priors derived by pipeline emission rates from NS2A only. Priors do not account for CH_4 dissolution and oxidation. • Transport model operated at coarse resolution (1°), unlikely to resolve the fine-scale transport of the three plumes near the source. • Effect of buoyancy on plume height at the point of release not considered[h]. *Comments* • Observations used: BIR, NOR and ZEP (ICOS) and Kjeller (NILU). • Considers inversion uncertainties by including forward and backward simulations. • Simulated well-mixedness in the planetary boundary layer (PBL) reduces the uncertainty on initial injection height in the modelling.
Inversion 2 *This study*	217–317 kt Atmospheric emissions quantified to: 30/09/22 22:00.	Tall tower inversion modelled using FLEXPART[65] to derive total atmospheric CH_4 emissions.	*Limitations* • Plumes are sparsely detected by the tall towers. Modelling is heavily dependent on the temporal profiles of the prior. • Error in the transport model is introduced due to meteorological uncertainty, including parametrisation of small-scale mixing processes, and changing planetary boundary layer (PBL) heights. • Effect of buoyancy on plume height at the point of release not considered[h]. *Comments* • Revision to ref. 18 estimate. • ICOS stations used: BIR, NOR and ZEP and Kjeller (NILU). • Uses updated Level 2 ICOS data released in 2023 that incorporates steep CH_4 concentration peaks. • Uses P-NAER$_{NSx}$ and C-NAER$_{NSx}$ emission profiles and priors. • Improved transport model resolution (0.2°) compared to ref. 18, allowing improved resolution of the plume transport. ZEP times series being better represented than HTM (which is excluded from the inversion) illustrates the importance of wind assimilation in addition to resolution. • Considers transport uncertainties addressed by comparing integrated signals (Methods). Transport error assessed by multiple model simulations (ECMWF at 1°, NCEP 0.5° degrees and WRF at 5 km). • Considers inversion uncertainties by resampling time series from different stations. • Simulated well-mixedness in the PBL reduces the uncertainty on initial injection height in the modelling.
Inversion 3 *This study*	≥230 kt Atmospheric emissions quantified to: 01/10/22 00:00.	Tall tower inversion modelled using ICON-ART[70,71] to derive a minimum estimate of total atmospheric	*Limitations* • Plumes are sparsely detected by the tall towers. Modelling is heavily dependent on the temporal profiles of the prior. • Effect of buoyancy on plume height at the point of release not considered[h]. • Due to large meteorological uncertainties in the ICON-ART model, estimate restricted to providing a lower bound of atmospheric CH_4 emissions (Methods). *Comments* • Uses ICOS stations BIR, NOR, HTM and UTO, and NILU station at Kjeller.

Method[a]	Estimate[b]	Description	Limitations & Comments
		CH_4 emissions.	• Uses updated Level 2 ICOS data released in 2023 that incorporates steep CH_4 concentration peaks. • Accounts for meteorological uncertainties using an ensemble of 40 ICON-ART forecasts, including an additional deterministic forecast. • Uses P-NAER$_{NSx}$ as a prior. • Considers three-dimensional CH_4 concentration field at fine resolution (6.5 km).
Inversion 4 *This study*	410±19 kt Atmospheric emissions quantified to: 01/10/22 00:00.	Tall tower inversion modelled using STILT[73,74] to derive total atmospheric CH_4 emissions.	*Limitations* • Plumes are sparsely detected by the tall towers. Modelling is heavily dependent on the temporal profiles of the prior. • Effect of buoyancy on plume height at the point of release not considered[h]. • Meteorological uncertainty is assessed using only one GFS forecast (c.f. Inversions 3,6). *Comments* • Revision of M2 estimate in ref. 8. • ICOS stations used: BIR, NOR, HTM and UTO. • Uses updated Level 2 ICOS data released in 2023 that incorporates steep CH_4 concentration peaks. • Uses P-NAER$_{NSx}$ as a prior.
Inversion 5 *This study*	740±134 kt Atmospheric emissions quantified to: 03/10/22 00:00.	Tall tower inversion modelled using LOTOS-EUROS[78,79] to derive total atmospheric CH_4 emissions.	*Limitations* • Plumes are sparsely detected by the tall towers. Modelling is heavily dependent on the temporal profiles of the prior. • Effect of buoyancy on plume height at the point of release not considered[h]. • Final analysis shows that the LOTOS-EUROS transport model is less-suited to this particular case study due to a tendency to overfit emissions to sparse observations. This introduces a positive bias to the results (Supplementary Discussion 4). • Uncertainty represents the standard deviation across fittings, which likely underestimates the uncertainty in the estimate. *Comments* • ICOS stations used: BIR, NOR and HTM. • Uses updated Level 2 ICOS tall tower data released in 2023 that incorporates steep CH_4 concentration peaks. • Uses P-NAER$_{NSx}$ and C-NAER$_{NSx}$ priors.
Inversion 6 *This study*	155–450 kt Atmospheric emissions quantified to: 03/10/22 23:00.	Tall tower inversion modelled using CHIMERE[82] to derive total atmospheric CH_4 emissions.	*Limitations* • Plumes are sparsely detected by the tall towers. Modelling is heavily dependent on the temporal profiles of the prior. *Comments* • Revision of the ref. 16 and 17 estimates. • ICOS stations used: BIR, NOR • Uses updated Level 2 ICOS data released in 2023 that incorporates steep CH_4 concentration peaks. • Uses C-NAER$_{NSx}$ as a prior. • Accounts for vertical profiles of emissions at coarse resolution (every ~10hPa) derived from CATHARE velocity rates at the break, as well as gas density after release in the atmosphere with regards to atmospheric stability at the leak sites. • Accounts for meteorological uncertainties using an ensemble of 11 ECMWF forecasts and quantifies these uncertainties using a Bayesian data assimilation approach.

Method[a]	Estimate[b]	Description	Limitations & Comments
Tall tower inversion ensemble *This study*	430±216 kt Atmospheric emissions quantified from: 30/09/22 22:00 to 03/10/22 23:00.	Mean estimate of tall tower inversion ensemble using Inversions 2, 4, 5 & 6.	*Limitations* • Assumes equal performance across inversion frameworks undertaken using a range of methodologies (i.e., differences in ICOS time series data, background definition, transport models and their resolution and meteorological data). Estimate quantifies a range of uncertainty obtained for an ensemble of models. *Comments* • Estimates are derived using a unified emission prior that accounts for marine dissolution and oxidation of CH_4. • Wide range of estimates illustrates the challenges of modelling the regional transport of an intense plume over large distances using sparse observations. • Large differences between this ensemble estimate and individual initial inversion estimates[8,15-18] highlights the strong dependence on priors when observations are sparse. • Transported plumes were narrow because each leak site was a strongly emitting and highly localized point source. Consequently, small changes in the advecting field caused the plumes to move away from the ICOS stations, particularly for those located nearby to leak sites. • Inversion frameworks typically optimize the posterior by applying changes where the uncertainties are large. In the absence of observations (the plume not passing over any of the tall towers) the models do not have a strong constraint during these periods. • Observations were taken continuously under most atmospheric conditions (e.g., no reliance on clear skies and daylight; c.f. satellite approaches[8,12,13]) when the plumes were transported over the stations.
Integrated atmospheric emissions estimate[i]			
Combined pipeline and marine emissions estimate *This study*	465±20 kt	Atmospheric CH_4 emissions derived in this study using modelled pipeline emission rates in conjunction with marine dissolution, outgassing and oxidation estimates.	*Limitations* • No TD quantification of CH_4 oxidation available. Thus, the estimate is reliant on the percentage of oxidation (~1%) estimated from BU subsea plume modelling[39]. *Comments* • Estimate derived using all available spatiotemporal data from the event, which are qualitatively assessed for their ability to provide a reliable estimate of different emission components. • Analysis provides a process-level understanding of the emission event from initial release over physical and biochemical processes in the water column through to sea-air gas exchange. • Demonstrated consistency with point-in-time TD emission rate estimates derived from satellites (Fig. 3). • Demonstrated broad consistency with cumulative estimates derived from satellites, and a tall tower inversion ensemble incorporating revised priors (Fig. 4).

[a]Includes reference and publication date. [b]Where applicable, includes the data acquisition period and corresponding period over which the estimate is valid. Dates are provided in the format dd/mm/yy hh:mm UTC. [c]Pipeline estimates correspond the amount of CH_4 contained in or released from the pipelines. In cases where initial and final pipeline pressures are not

reported, we assume the estimate corresponds to the CH_4 contained in the pipelines prior to rupturing. In cases where initial and final pipeline pressures are reported, we assume the estimate corresponds to the CH_4 released from the pipelines. [d]We estimate 501 kt from the natural gas volumes (778 Msm^3) reported by ref. 5, assuming the natural gas contains 93% CH_4 by mass and had a CH_4 density of 0.693 kg/m^3 at 20°C and 1 atmosphere. [e]Marine estimates correspond to the amount and/or rates of CH_4 dissolution, oxidation and sea-surface outgassing in/from the Baltic Sea. [f]Although an estimate of 10–55 kt dissolved CH_4 is reported in ref. 10, we assess that 10 kt dissolved CH_4 is a more reliable estimate. See main text and *Comments* for details. [g]Airborne, satellite and tall tower estimates correspond to the cumulative amount and/or rates of CH_4 emission to the atmosphere. [h]Leads to uncertainty in the appropriate height to use in the model to represent the source due to the uncertainty in the velocity and buoyancy of the plume as it enters the atmosphere. [i]Estimate quantifies the total amount of CH_4 emitted to the atmosphere from the three ruptured pipelines.

Supplementary Discussions

Supplementary Discussion 1 | Impact of northern NS2A partial rupture on modelled pipeline emission rates

We did not model emission rates from the northern NS2A leak site using PBREAK and CATHARE. The leak was caused by a small partial break in the pipeline[31], resulting in only a small visible sea foam patch at the leak site[117]. Moreover, as we do not have any data on the break size and its dimensions, we did not model the resulting emission rates using PBREAK and CATHARE. It is also worth noting that satellite imagery over the northern leak sites on 29 September and 1 October did not detect any CH_4 enhancement over the northern NS2A leak site[8]. For these reasons, we expect that the northern NS2A leak is likely to only have a negligible effect on the emission rates from the southern NS2A leak site. However, it could partly explain why some satellite emission rate estimates for the southern leak are lower than predicted by P-NAER$_{NS2A}$ and C-NAER$_{NS2A}$ in Fig. 3 and Extended Data Table 4. We note that a second rupture impacts only the duration of the release, and not the amount released from the NS2A pipeline.

By comparing the size of the area of sea above the leaks that were affected by the pipeline blowout at both the northern and southern NS2A leak sites, ref. 3 estimates that approximately 89% of emissions from NS2A were emitted from the southern leak site. This approach assumes there is a correlation between the emission rates and the size of the disturbed sea surface. Whilst we do not attempt to validate this approach using data within our paper, we provide comparisons of satellite estimates[8,12,13] to P-NAER$_{NS2A}$ and C-NAER$_{NS2A}$ adjusted by a factor of 0.89 in Extended Data Table 4. The emission rate for the S-2B observation of 72±38 t/hr is within the uncertainty of the adjusted P-NAER$_{NS2A}$ (77–102 t/hr), as well as the adjusted C-NAER$_{NS2A}$ (104–174 t/hr). The emission rate for the L8 and S-2B ensemble of 502±464 t/hr is within the uncertainty of the adjusted P-NAER$_{NS2A}$ (76–230 t/hr), as well as the adjusted C-NAER$_{NS2A}$ (104–310 t/hr). The emission rate for the GHGSat-C1 observation of 84±24 t/hr is within the uncertainty of the adjusted P-NAER$_{NS2A}$ (75–101 t/hr), as well as the adjusted C-NAER$_{NS2A}$ (104–174 t/hr). The emission rate for the GHGSat-C4 observation of 24±8 t/hr is still lower than the adjusted P-NAER$_{NS2A}$ (64–90 t/hr), as well as the adjusted C-NAER$_{NS2A}$ (93–162 t/hr).

Supplementary Discussion 2 | Methane hydrate formation

We use pressure, temperature, velocity, and Froude number[109] time series computed using CATHARE to assess whether CH_4 hydrate formation was possible during the Nord Stream pipeline decompressions. Our simulations indicate that natural gas temperatures at the rupture points could have reached a minimum of -85°C (for NS1A and NS1B) and -72°C (for NS2A) during the decompression (Supplementary Fig. 1), assuming no heat transfer during expansion. Phase diagrams of CH_4 hydrate stability suggest that under these conditions, CH_4 hydrate and water ice formation are possible[118]. However, CH_4 hydrate formation can only occur when both the natural gas and water are in contact under hydrate forming conditions. In the case of the Nord Stream pipeline leaks, this could occur: (1) where the gas leaves the pipeline and is injected into the water column; (2) within the pipelines themselves if seawater had entered; and/or (3) within the pipelines if the natural gas contained water. We assess the possibility of each scenario below.

(1) Once emitted from the pipeline, the natural gas will very quickly warm with only minor change of the temperature of the water because of the far higher heat capacity of the water per volume in comparison to natural gas – a factor of ~210 to ~330 larger per volume depending on the temperature at the break[54]. Thus, if CH_4 hydrate did form, it would be subject to the transfer of heat from the surrounding seawater (~5°C) and exist for only a very short period before being reverted to a gaseous phase.

(2) Gas velocities at the rupture sites simulated using CATHARE were high (~10-300 m/s) during most of the pipeline decompressions. For example, our simulations indicate that <5 kt and <0.3 kt CH_4 was released from the northern and southern sections of the NS1A pipeline under break flow velocities <10 m/s, respectively (Supplementary Fig. 2). Moreover, <1kt and <0.1kt CH_4 was released from the northern and southern sections of the NS1A pipeline when the Froude Number was under one, respectively (Supplementary

Fig. 3). This indicates that seawater was unlikely to have entered the pipeline during most of the emission event, meaning that CH_4 hydrate formation due to seawater entering the pipelines would have been minimal.

(3) The natural gas contained within the pipelines was dry gas and is not expected to contain any significant amounts of water[34,108]. Thus, within the pipeline, hydrate and ice formation should be limited by the lack of water.

Overall, we conclude that the formation of CH_4 hydrate outside and/or within the pipeline would not have a significant impact on the rate of methane emitted from the pipelines and to the atmosphere. In addition, liquid methane formation is not expected under the conditions derived by our CATHARE simulations. This indicates the CH_4 would have been in a gaseous phase during the entire emission event.

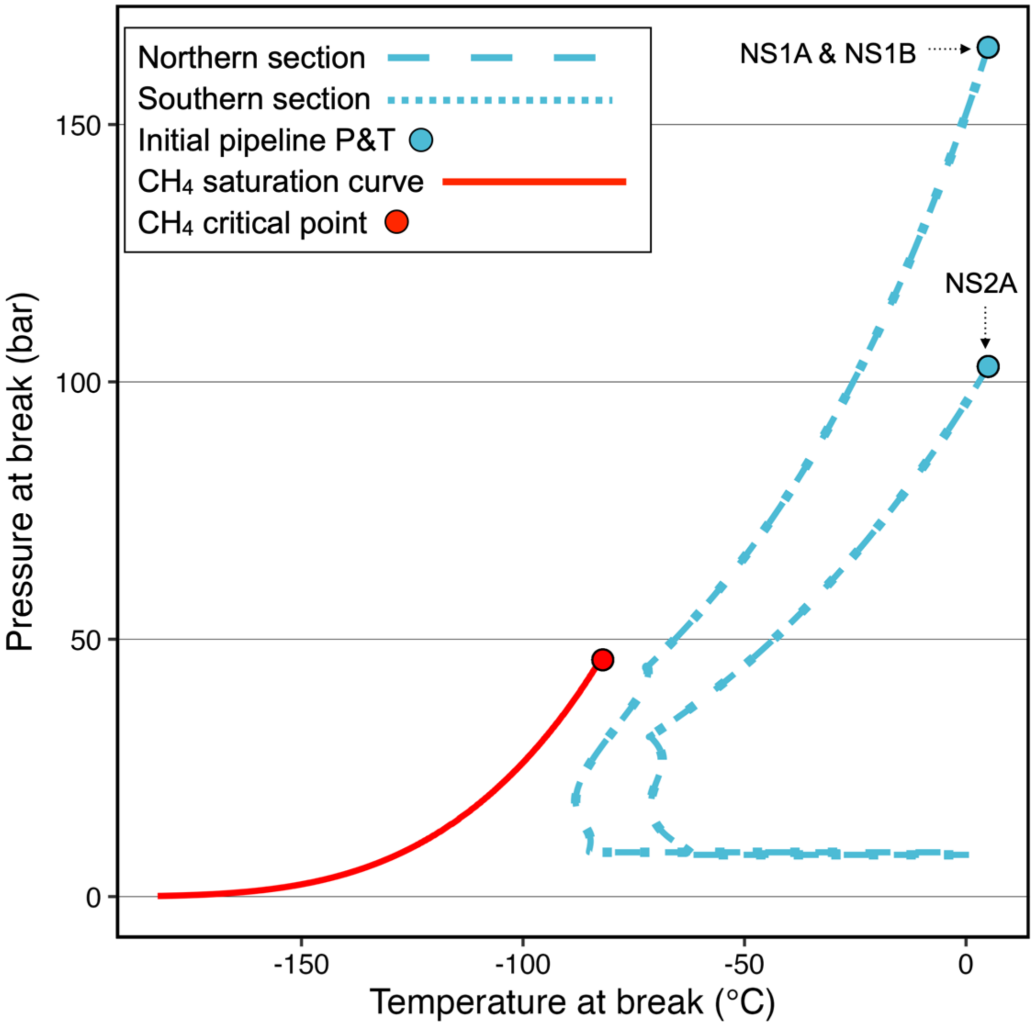

Supplementary Fig. 1 | Time series of pressure and temperature at the pipeline breaks for NS1A, NS1B and NS2A obtained using CATHARE. The CH_4 saturation curve[54] is also shown to demonstrate that no liquid CH_4 formation occurred during the leaks. Simulation differences between Northern and Southern sections are minor, and therefore both lines overlap.

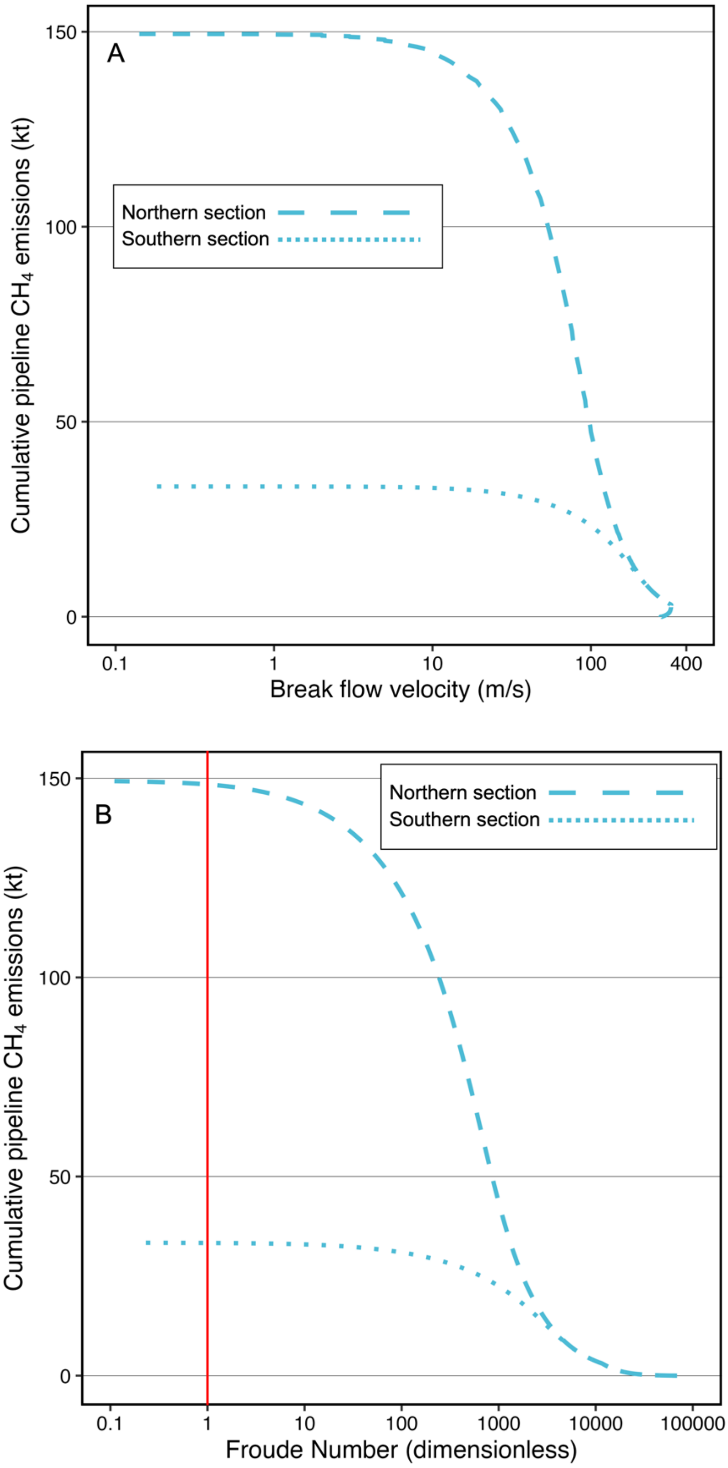

Supplementary Fig. 2 | Cumulative pipeline CH_4 emissions compared to (A) break flow velocities, and (B) Froude numbers, simulated for the NS1A pipeline sections using CATHARE. Froude numbers >1 (to the right of the red line in (B)) indicate that the break flow inertia is enough to prevent seawater entering in the pipeline.

Supplementary Discussion 3 | Equation of State (EOS) in PBREAK and CATHARE

PBREAK and CATHARE, like other flow dynamic simulation tools, use an Equation of State (EOS) to compute fluid properties and evaluate fluid density. Many different EOS are present in the literature: some are simple (such as the ideal gas law), and some are more complex and more accurate. For natural gas, the reference EOS is GERG-2008[55] used in Standard Reference Database 23, Reference Fluid Thermodynamic and Transport Properties (REFPROP) of the National Institute of Standard and Technology (NIST)[54]. GERG-2008 computes natural gas properties for a given gas composition using complex formulas. Unfortunately, it was not possible to use GERG-2008 EOS with the exact natural gas composition in our PBREAK and CATHARE computations:

- PBREAK uses a simplified EOS, which results in a total cumulative mass discrepancy of ~3% (Extended Data Table 3).
- CATHARE uses GERG-2008 EOS but with a simplified gas composition (neglecting components in the mixture that make up less than 0.1%), which results in a total cumulative mass discrepancy of ~0.3 % (Extended Data Table 3).

Supplementary Discussion 4 | Over-fitting of atmospheric emissions in Inversion 5

Due to the sharp and rapid variations in emission rates from the leaks, the LOTOS-EUROS[78,79] (LE) fitting routine used in Inversion 5 could not be matched exactly with peaks observed at the BIR and NOR stations. Supplementary Fig. 3 shows an LE model run without the Nord Stream pipeline leak emissions (in red) and with the P-NAER$_{NS2x}$ prior (in blue) for the BIR (Supplementary Fig. 3a), NOR (Supplementary Fig. 3b) and HTM (Supplementary Fig. 3c) stations. There are not many occasions where the modelled plume from the leaks is above the baseline (red) at all stations. At the NOR station, the observational data aligns with a simulated emission peak using P-NAER$_{NS2x}$ as the emission prior on 27 September, but not over the entire duration of that observed peak. In the LE fitting procedure, the emissions will be scaled upwards to match observations better. With very limited observations, this leads to an overestimation of atmospheric emissions.

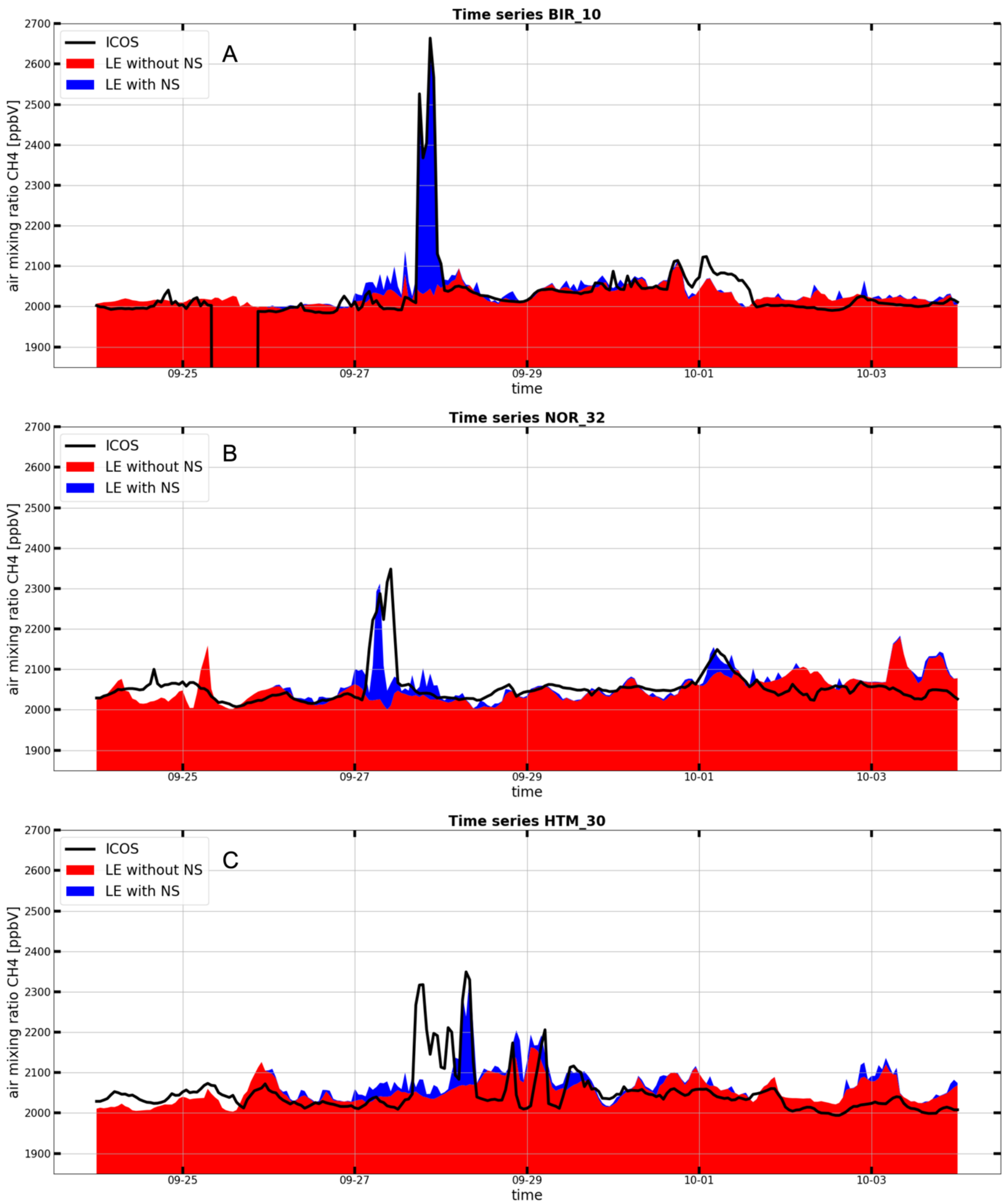

Supplementary Fig. 3 | Time series of an LE model run without the Nord Stream pipeline emission rates (in red) and with the P-NAER prior (in blue) for the BIR[76] (A), NOR[63] (B) and HTM[77]Error! Reference source not found. (C) stations.

Supplementary Methods

This section provides brief method descriptions of the bottom-up pipeline emission rates simulations we performed in our study (Supplementary Method 1), as well as the top-down methods used to estimate CH_4 emissions in the Baltic Sea and atmosphere from the Nord Stream pipeline leaks (Supplementary Methods 2-7). For a complete overview of each top-down method, the relevant publication should be consulted.

Supplementary Method 1 | Pipeline emission simulations

When a break occurs in a pipeline, gas is released into the surrounding environment and the pressure in the pipe in the vicinity of the break drops. This results in a pressure wave which propagates along the pipeline away from the break at the speed of sound. The gas flow from either side of the break will be balanced immediately following the rupture. However, at later stages, the flows decay with time independently on each side at rates determined by the pipeline system, and typically will become increasingly unbalanced during the event. This is affected by features such as locations of compressor stations, and feeds from or to other pipelines, which may be at large distances from the failure point. These upstream and downstream boundary conditions determine whether the flow through the pipeline at the rupture will decrease to zero or to a steady-state flow rate.

PBREAK

PBREAK is a mathematical model used to simulate the outflow of gas following the sudden puncture or rupture of a high-pressure transmission pipeline[36,47-49]. The model is embedded in the PIPESAFE Quantitative Risk Assessment software and is owned by a group of worldwide natural gas transmission companies and the software developer DNV. The model comprises a set of non-linear equations accounting for continuity and mass balance, momentum, and energy following a pipeline rupture, which are solved using an implicit finite difference scheme. The natural gas is modelled as a real gas with the propagation of the expansion wave following a rupture modelled adiabatically in a single straight pipe. The effect of friction is considered in both the energy and momentum equations embedded in the software. The connection of a pipeline to the rest of the transmission network can be defined by one of four boundary conditions: *no flow*, *constant pressure*, *constant flow*, or *constant volume*. In this case, the applicable boundary condition is *no flow*, because flow valves were closed on each side of the pipelines at the time of failure. At the rupture point, the boundary condition is that the flow speed is sonic if the pressure at the exit is greater than the external pressure. If the outflow is choked, the gas outflow rates will be governed by internal pressure and hole size, in which case the external pressure (i.e., the main difference between an onshore and an offshore pipeline) will have no effect on the predicted outflow rate. The outflow will stop being choked when the pressure in the pipeline drops to around double the external pressure. Water depth can be specified in the PBREAK model setup, meaning it can consider the correct external pressure when modelling subsea pipeline ruptures. This consists of the atmospheric pressure plus the pressure head of the water above the pipeline.

The PBREAK model has been validated against experimental data obtained in a large-scale experiment modelling the emission rates of natural gas from the rupture of a 77 km long pipeline measuring 914 mm external diameter under 60 bar[48]. PBREAK has also been applied as a risk assessment tool for the potential rupturing of a natural gas pipeline within a major river crossing[49].

CATHARE

The CATHARE code was developed by the French Alternative Energies and Atomic Energy Commission (CEA) and is used for the thermal hydraulic simulation of multiphase flows[37,51-53]. The current version of the code is CATHARE-3[37]. CATHARE has been extensively used to model break flows from pipes in pressurised water reactor (PWR) accidents[51,52]. Although originally developed to simulate two-phase flows of water or other nuclear coolants, the code has been extended to non-nuclear applications[50]. CATHARE has an extensive validation matrix with calculations performed on more than 40 experimental benches and comparison of results from approximately one thousand tests[51,52]. As part of our study, we perform additional computations to validate its usage as a simulation tool capable of simulating single-phase gas pipeline ruptures.

In Supplementary Fig. 4, we compare simulated pipeline pressures obtained using CATHARE with experimental pressure data at four positions along a tube undergoing depressurization[119]. The pressure evolution computed using CATHARE shows excellent agreement with the ref. 119 experimental data. This test case allows us to verify that keeping a very small time-step throughout the transient, and a small mesh size along the pipe, is necessary to simulate the propagation of the pressure wave – but is not a necessary condition to predict accurately the evolution of the outlet flow.

In Supplementary Fig. 5, we compare choked flow rates of Nitrogen and Oxygen through a conical convergent-divergent nozzle simulated using CATHARE with those derived experimentally in the experimental database in ref. 120. Computed mass fluxes using CATHARE show good agreement with those in the experimental database. Since the transients from pipe breaks often lead to the occurrence of choked flows, the ability to accurately predict sonic flow rate is an important requirement for a thermal-hydraulic system code such as CATHARE[121]. This additional validation indicates CATHARE can simulate monophasic choked flow from a ruptured pipeline. The choked mass fluxes we selected in the ref. 120 database are within the range of those simulated for the Nord Stream pipeline leaks, which reached up to ~20,000 kg/s/m^2 for the NS1 pipelines and ~12,000 kg/s/m^2 for the NS2A pipeline.

In Supplementary Fig. 6, we compare computed pressure profiles obtained using CATHARE with experimental pressure data on steady state critical flowrate in tubes with large length over diameter (L/D) ratios[122]. We selected eight tests with monophasic conditions from the ref. 122 experimental database. CATHARE shows good agreement with the experimental values. This indicates CATHARE can accurately predict pressure loss under choked condition in tubes with very large L/D values. The L/D ratio in the ref. 122 experimental database (~16,000) is low compared to the Nord Stream pipelines (~10^6 for northern side and ~10^5 for southern side) but it is one of the largest found in the literature.

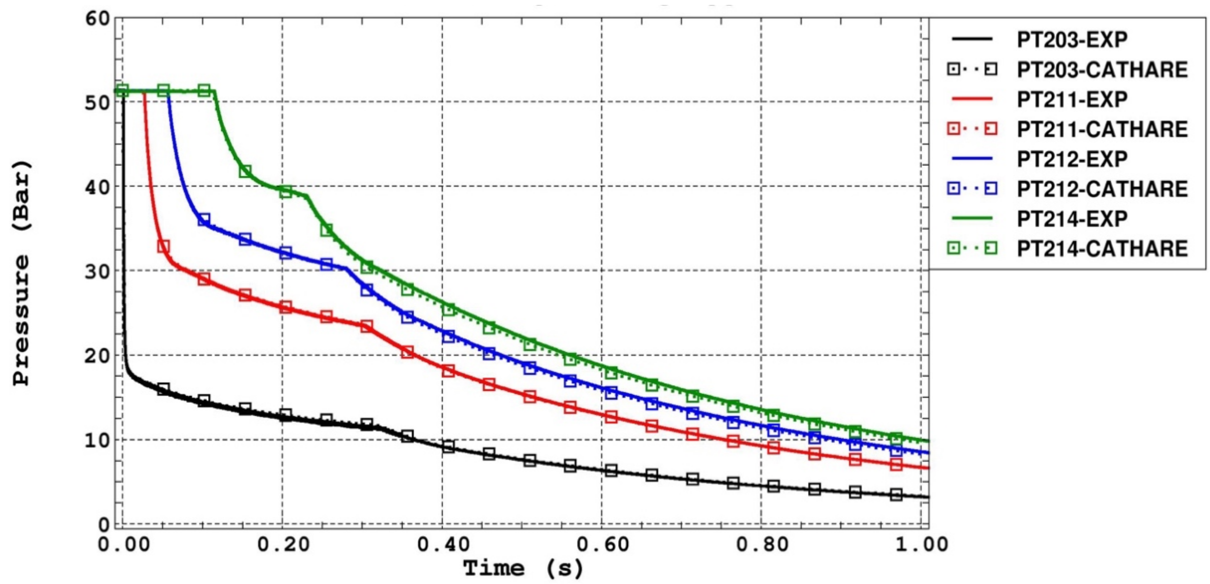

Supplementary Fig. 4 | Comparison of simulated pipeline pressures obtained using CATHARE (dotted lines and squares) with experimental pressure data (full lines)[119] at four positions along a pipeline undergoing depressurization: PT203, PT211, PT212 and PT214 (0.28 m, 9.595 m, 29.986 m and 39.984 m from the break, respectively).

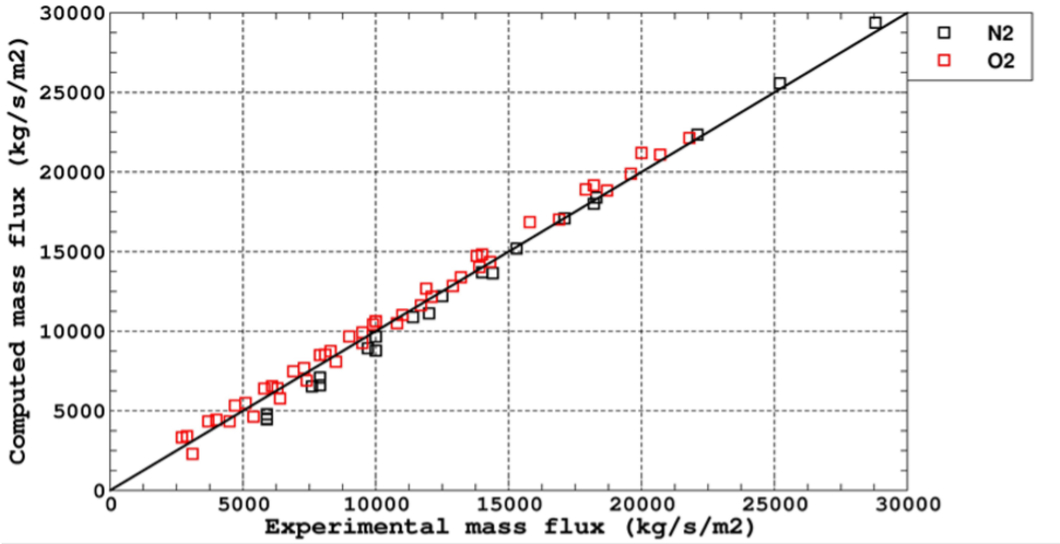

Supplementary Fig. 5 | Comparison between computed choked flow rate values obtained using CATHARE and experimental data[120] on the steady state critical flow rate of Nitrogen (black) and Oxygen (red) fluids.

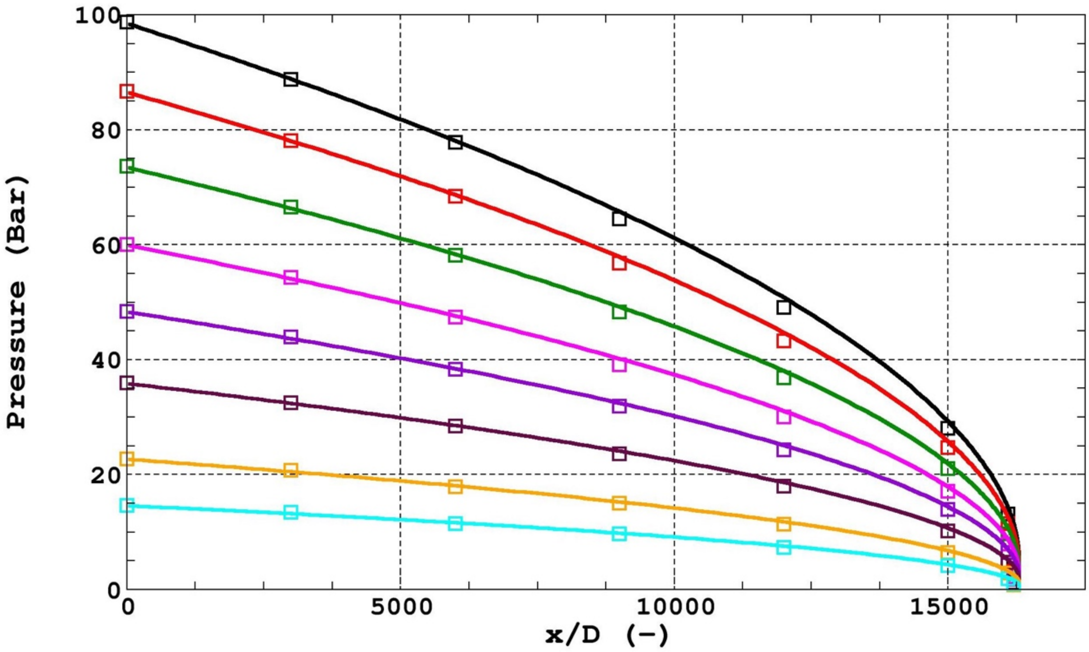

Supplementary Fig. 6 | Comparison of computed pressure profile obtained using CATHARE (solid lines) with experimental pressure data (squares)[122] on steady state critical flow rate in tubes with large length over diameter (L/D) ratios. Each colour in the figure corresponds to a test case.

Additionally, we use CATHARE results to compute the evolution of the Froude number[109] (Fr) at the break using Eq. SI-1:

$$Fr = \frac{V_{Break}^2}{g\ D\ \frac{\rho_{Water} - \rho_{NG}}{\rho_{NG}}} \quad \text{(Eq. SI-1)},$$

where g is gravity constant (9.81 m/s²), D is the pipeline diameter (1.153 m), V_{Break} is the natural gas velocity at the break (m/s), ρ_{NG} is the natural gas density at break (kg/m³) and ρ_{Water} is the seawater density (1000 kg/m³). This Froude number is the ratio between the natural gas flow inertia at the break and the seawater gravity force field. A Froude number greater than one indicates that the break flow inertia is enough to prevent seawater entering in the pipeline (see also Extended Data Fig. 3 and Supplementary Discussion 2).

CATHARE model sensitivity

In addition to assessing the influence of temperature, depth, pipeline section lengths and natural gas composition, we assessed the sensitivity of the CATHARE code to the choice of pipeline roughness coefficients, heat transfer coefficients, mesh number and orifice size (Supplementary Methods Table 1). In Supplementary Fig. 7, we show an example of the sensitivity of our break flow rates to these model variables for the northern and southern sections of the NS1A pipeline.

Supplementary Methods Table 1 | CATHARE model sensitivities and their maximum effects on simulated flow rates for NS1A, NS1B and NS2A.

Variable	Values tested	Maximum absolute deviation for flow rates >100 t/hr (t/hr CH_4)	Maximum absolute deviation for flow rates >100 t/hr (% of flow)	Maximum absolute deviation for flow rates <100 t/hr (t/hr CH_4)	Maximum absolute deviation for flow rates <100 t/hr (% of flow)
Heat transfer coefficient between external wall layer and the Baltic Sea ($W/m^2/K$)	0 10^6	1 6	1.9 0.9	1 2	24.2 5.5
Multiplication coefficient for heat transfer coefficient between internal wall layer and the natural gas	0.1 10	88 163	0.5 0.8	4 <1	15 1.7
Pipeline roughness multiplication coefficient	1/15 5	1147 835	8.9 6.1	19 33	80 137
Mesh number	×~2[a]	7	0.2	<1	1.3
Break Section	0.81[b]	2185	10.2[c]	<1	0.5

[a]No precise number is used because the meshing depends on the pipeline part considered. [b]Break size was multiplied by 0.9, equivalent to the break section being multiplied by a factor of 0.81 (0.9×0.9). [c]Note the maximum absolute deviation occurs within 1min of the rupture. After 1min, absolute deviations in the flow rate are <1% of flow.

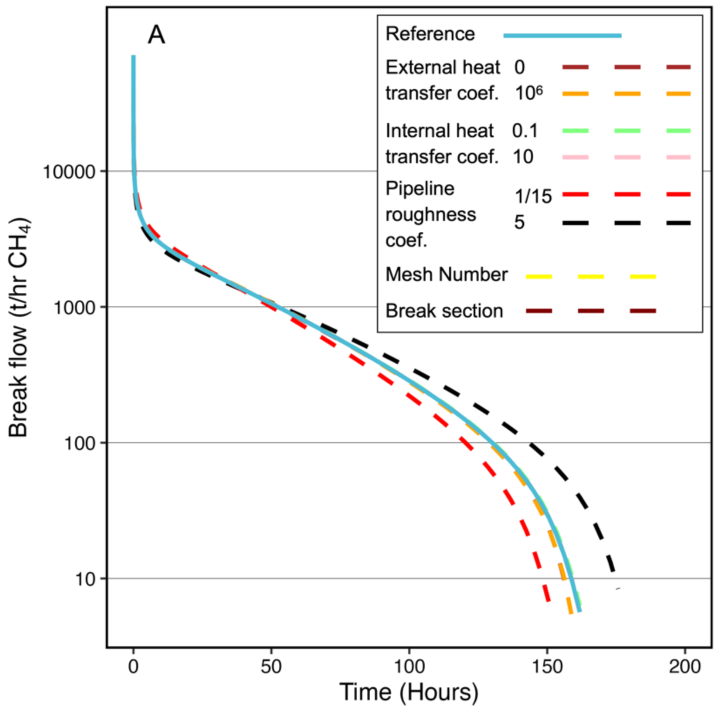

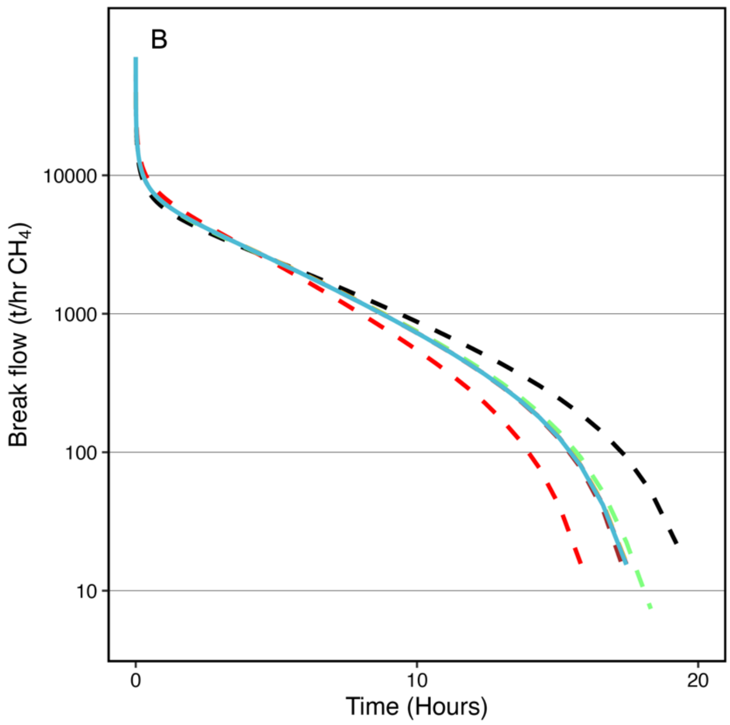

Supplementary Fig. 7 | Sensitivity of NS1A break flow rates for the (A) northern and (B) southern pipeline sections to the choice of external and internal pipeline heat coefficients, pipeline roughness, mesh number and break section used in the CATHARE simulations.

Across all three pipelines and for flow rates >100 t/hr CH_4, the most influential parameters over the flow rate are the pipeline roughness multiplication coefficient and break section (Supplementary Methods Table 1). The choice of pipeline roughness coefficient leads to a maximum absolute deviation of 1147 t/hr CH_4, equivalent to 8.9% of the flow rate at the time. In percentage terms, flow rates become increasingly sensitive to the pipeline roughness coefficient as flow rates decrease, however their relative difference become smaller (e.g., a maximum difference of 33 t/hr for flows < 100 t/hr). The size of the break section leads to a maximum absolute deviation of 2185 t/hr CH_4, equivalent to 10.2% of the flow rate at the time. However, the influence of the break section decreases substantially after 1 min, and absolute deviations in the flow rate are <1% of flow for the remainder of the release. Using twice as many meshes has a minor effect on simulated flow rates. The choice of both internal and external heat transfer coefficients has only minor effects on simulated flow rates when >100 t/hr. These effects become more pronounced in percentage terms with flows <100 t/hr, however these correspond to only a maximum relative deviation of 4 t/hr from the reference case.

Supplementary Method 2 | Ocean glider and ship of opportunity measurements

From 5 October 2022 to 2 January 2023, dissolved CH_4 concentrations were observed continuously along a transect at the north-eastern side of the northern leaks by SeaExplorer gliders[9]. The transect was chosen because it was downwind and downstream of the leaks, just outside of a 5 nm wide exclusion zone prohibiting access close to the leak sites. The gliders were also equipped with CTD and oxygen sensors that recorded at 1 Hz, which corresponds to ca. 10 cm vertical resolution. To improve accuracy, the CH_4 sensor was calibrated prior to and after the observation period for a range of 10 nM – 1 μM.

The ship of opportunity (SOOP) Finnmaid (DE-SOOP-Finnmaid), equipped with instrumentation for continuous detection of surface partial pressures of CH_4 and carbon dioxide as part of the European ICOS Research Infrastructure, traversed the Bornholm Basin close to the leak sites 2 times every 3 days. The instrumental setup and underlying calculations have been described in detail in ref. 123 and references therein. In brief, water is pumped continuously into a shower-type air-water equilibrator, and the mole fraction of CH_4 (and carbon dioxide; CO_2) in the gas are detected using a Los Gatos Research CH_4/CO_2 gas analyser. By using a set of auxiliary parameters, the data are converted to partial pressures using the total gas pressure and reported as concentration based on the *Bunsen* solubility coefficients determined by ref. 124. Three reference gases provided by the ICOS Calibration lab were used for calibration.

The glider and SOOP observations served to describe the vertical and horizontal plume structure and establish initial conditions for a model. A numerical Lagrangian chemical fate and transport model[125] was used to simulate the CH_4 spread and was driven by both PREAK and CATHARE emission rate data presented in this study. The Baltic Sea Physics Analysis and Forecast model[126] and wind fields from ERA5 were used to model advection/diffusion and outgassing of CH_4. By iterative linear regression between modelled and observed concentrations, 9–15 kt of dissolved CH_4 was quantified. Based on the model's two-dimensional surface concentration fields, outgassing rates were also calculated. Resulting surface outgassing flux rates are up to 74 t/hr CH_4. A total of 8–13 kt CH_4 was outgassed from 26 September 2022 to 1 January 2023. This suggests that the majority of the dissolved CH_4 had been outgassed by January 2023. The methods and results of this work are detailed further in ref. 9.

Supplementary Method 3 | Discrete water sampling using CTD casts & ship-based sea-air flux estimates

Discrete samples of CH_4 and its stable carbon isotopic signature ($\delta^{13}C\text{-}CH_4$) were acquired in the seawater column between 3 and 5 October 2022, and again between 9 and 12 January 2023, onboard RV Skagerrak[10]. Sampling locations with $\delta^{13}C\text{-}CH_4$ values above -40‰ were used to distinguish locations where there was a clear presence of fossil CH_4. An average CH_4 concentration of 3500 nM, and a maximum concentration of 20000 nM, was measured across sampling locations. From average and maximum concentrations, it was estimated that 0.8 and 4.5 kt CH_4, respectively, was dissolved in an area covering 300 km^2 and water depths up to 50 m. Using Lagrangian particle simulations released at the rupture sites in conjunction with hourly currents from the Copernicus Marine Data Store (MDS) Baltic Sea Physics Reanalysis[127], it was estimated that the observations comprised only 9% of the actual modelled plume released from the pipelines. Accordingly, the amount of CH_4 in the water column was extrapolated to be 10 kt CH_4 based on average CH_4 concentrations, and 55 kt CH_4 based on the maximum dissolved CH_4 concentration. The highest dissolved CH_4 concentrations were measured between 30-50 m depth, which is below the mixed surface layer, and in a well stratified layer between the thermocline and halocline. There were some indications in the CTD profiles that water was mixed at the release sites (due to the violent gas release) and interlayered at 30-50 m depth. Thus, after the mixing at the release site, natural convection was unlikely to impact on the concentration before cooling in late autumn/winter.

Atmospheric CH_4 concentrations were measured onboard RV Skagerrak near several CTD sampling sites using a Picarro G2132-i laser spectrometer. Using continuous ship-based measurements of wind speed, atmospheric CH_4 concentrations were converted to CH_4 flux rates using the air-sea flux exchange equations derived from ref. 128. Estimated sea-surface CH_4 outgassing rates ranged from $0.5\text{–}5\times10^{-3}$ t/hr/km^2. Regional modelling of these flux rates has not been undertaken. Analysis of results from a second campaign between 9 and 12 January 2023 are pending. Initial data indicates CH_4 concentrations returned to background levels by early January 2023 in the absence of a thermocline. These data also show isotopic enrichment, indicating that oxidation of the CH_4 has occurred. The results of the first campaign are detailed in ref. 10.

Supplementary Method 4 | Airborne observations using HELiPOD

Atmospheric CH_4 mixing ratios were obtained locally at the leak sites during two campaigns: one on 5 October 2022 and one on 16 and 17 November 2022[11]. In the October campaign, CH_4 measurements were obtained with a Picarro G2401-m and a Li-Cor LI-7700. The platform was the HELiPOD, a drag sonde flown as an external sling load attached to a helicopter[41]. The helicopter, type Airbus H125, was operated by the company Helipoland. Two flights each were performed in each campaign. All flights started from Kołobrzeg, Poland. Considering the available flight duration of approximately 3 h, the first flight path on 5 October was designed to capture CH_4 mixing ratios both upwind and downwind of the multiple leak sites northeast of Bornholm and determine the atmospheric boundary layer height. Based on the spatial pattern of CH_4 enhancements observed during the first flight, the second flight was designed to increase the spatial coverage southwest (upwind) of the Northern leak sites and include a downwind leg of the leak site southeast of Bornholm. Together, the two flights covered an area of about 70 km along-wind and 20 km across around the Northern leaks and the area between Northern and Southern leaks. The flights in November focused less on the leak sites themselves but covered a wider area to capture potential emissions from the expected wider distribution of dissolved CH_4.

To date, analyses were focused on calibrated data obtained with the Picarro instrument on 5 October 2022. Analysis of the data from the November 2022 campaign is pending. For each sounding, a surface influence function or “footprint” was computed using the model WRF-STILT, driven by ECMWF’s ERA5 weather reanalysis. The footprint is a map that quantifies the CH_4 enhancement at the observation location caused by a unit flux from a unit area at the surface. To reduce the impact of small-scale variability and computational cost, observations and footprints were averaged over 20 second intervals.

Observations and footprints were used to estimate surface-atmosphere emissions of CH_4 for 5 October 2022. Since emission estimation for an area source from atmospheric data is usually an underconstrained problem, the helicopter-borne data and footprints were used to optimise a prior emission estimate with a Bayesian optimisation technique. The prior estimate was set to zero throughout the domain. The specific optimization technique was geostatistical inverse modelling (GIM)[129]. Using this method, covariance matrices and optimized emissions were estimated on a $(1/120)° \times (1/80)°$ grid. The optimization was constrained to non-negative solutions. Emission rates between 19–48 t/hr CH_4 were estimated for 5 October 2022. The methods and results of this work are detailed further in ref. 11. Forthcoming results of a second airborne campaign on 16 and 17 November 2022 using HELiPOD would serve as further comparison with other modelled outgassing rates[9,10], but would not alter the atmospheric emissions budget we derive in Table 1.

Supplementary Method 5 | S-2B observations

Ref. 8 quantified CH_4 emissions from the southern NS2A leak site at 10:07 UTC on 30 September using the Sentinel-2B (S-2B) satellite. A Beer's law retrieval[130] and integrated mass enhancement method (IME)[42] were used to quantify emission rates. The first step was the derivation of the CH_4 concentration enhancement (ΔX_{CH4}) map based on the simple band ration between a band sensitive to CH_4 and a spectrally close band with no sensitivity (or minimum sensitivity). Then a plume mask was performed to select CH_4 plume pixels and quantify the emission. Finally, the selected pixels were converted into flux rate (Q) by applying the IME method. An emission rate of 72±38 t/hr was derived.

This estimate was published approximately one month after the leaks occurred, and therefore applied the standard emission retrieval for S-2B data. Accordingly, Ref. 8 noted that the spectral reflectance of the bubbles may have contributed a large fraction of the reflected radiance which is difficult to separate from the absorption of CH_4 in the SWIR band, potentially leading to an over estimation of ΔX_{CH4}. They also noted that the satellite images missed a large part of the plume because water can absorb most of the sunlight in the SWIR range used for CH_4 retrieval, especially for nadir observations using S-2B. These uncertainties are addressed later in the literature by ref. 12 (Supplementary Method 6).

Supplementary Method 6 | L8 and S-2B observations

L8 and S-2B satellite nadir observations of the southern NS2A leak were analysed by ref. 12 for 29 and 30 September 2022, respectively. These authors applied the Multi-Band Single-Pass (MBSP) method[43] to infer CH_4 enhancement over the southern NS2A sea foam patch. They then used the IME method[42] in an ensemble approach to estimate CH_4 emission rates and their uncertainties. However, this use-case challenges some of these methods' hypotheses: (1) based on these individual observations, MBSP cannot separate the spectral dependence of sea foam albedo from the CH_4 signal; and (2) the IME can only rely on a partial plume observation over the sea foam patch area. To circumvent these issues, the authors performed a two-fold custom calibration: (1) using sea foam observations by L8 and S-2B in boat trails to provide an empirical calibration of the sea foam albedo spectral dependence; and (2) by performing a custom IME effective wind calibration that accounts for the partial plume mask.

Ref. 12 report ensemble-average positive emission rates of 507±673 t/hr and 496±640 t/hr for L8 and S-2B, respectively. These large 1σ uncertainty intervals are mainly driven by the uncertainty of sea foam albedo spectral dependence calibration and include zero emissions. Assuming these estimates are independent, the average L8 and S-2B emission rate is 502±464 t/hr.

Supplementary Method 7 | GHGSat observations

Following reports of the Nord Stream gas leaks on 26 September 2022, GHGSat immediately began tasking its satellite constellation to detect and quantify CH_4 emissions from the offshore NS2A leak in the Baltic Sea[13]. The satellites contain imaging spectrometers based on wide angle Fabry-Pérot (WAF-P) technology using solar backscattered radiation in the short-wave infrared[131]. The instruments acquire several closely spaced images of a target as it pans through the field of view, and these are used to retrieve the CH_4 column density and emissions source rate. Using this targeted observation mode, the GHGSat constellation can detect CH_4 plumes with 25 m spatial resolution on land. For offshore measurements, however, GHGSat's conventional "nadir" observation mode is not sufficient due to the low levels of solar short-wave infrared radiation reflected from water surfaces. Instead, to capture sufficient signal, the observation viewing geometry is chosen such that the GHGSat instrument measures specularly reflected light from the sun close to the "glint" spot. In this sun glint observation mode, the viewing geometry is chosen to minimize the glint scattering angle and maximize the measured light signal.

For the Nord Stream gas leaks, while the first attempts by GHGSat and other satellites were unsuccessful due to cloudy conditions, three clear-sky opportunities on 30 September all yielded successful plume detections of the southern NS2 leak. Supplementary Methods Table 2 provides a summary of measurement parameters for each observation. The source rates are estimated using the IME method[42], and local wind speed is obtained from GEOS-FP. The estimated emission rates are 84 ± 24 t/hr for the C1 observation and 24 ± 8 t/hr for the C4 observation. Following the observations on 30 September, the next clear sky observation was on 3 October 2022. GHGSat satellites confirmed that the leak had stopped by this time.

The glint scattering angle quantifies how far the viewing angle is from the optimal "specular" angle for sun glint. In general, a small scattering angle translates to a higher signal at the detector, and this is reflected in the retrieved surface reflectivity near the source in Supplementary Methods Table 2. The C1 observation has the lowest scattering angle and the highest reflectivity of the three observations. Note that for specular reflections, the surface reflectivity can be larger than 1. GHGSat's standard criterion requires the scattering angle to be no more than 20 degrees. To maximize the number of measurement opportunities, GHGSat relaxed its standard acceptance criteria for the allowed glint scattering angle. The C2 and C4 observations both violate this criterion, which leads to low signal for both – especially for the C2 observation where the signal was more than 100 times lower than C1. GHGSat has not characterized and calibrated the detection system for very low signal levels. Therefore, a source rate estimate for the C2 observation is not provided. However, based on the spatial extent and shape of the signal, GHGSat are confident in the validity of the plume *detection*.

Supplementary Methods Table 2 | Summary of key parameters for the three detection events on 30 September 2022.

Time (UTC)	Satellite	Glint Scattering Angle (degrees)	Albedo/Surface reflectivity	Viewing zenith angle (degrees)	Ground sample distance (m)	Wind speed (m/s)	Estimated source rate (t/hr)
8:51:36	C2	45°	0.007	58.5	80	5.5	N/A
10:26:40	C1	10°	1.02	66.1	135	6.0	84 ± 24
12:54:34	C4	30°	0.04	65.6	100	5.5	24 ± 8

To view the glint spot, GHGSat oriented its satellites at high across-track and along-track angles. This can be seen in the high viewing zenith angles, which are at 58 degrees and above. The high angles are required to minimize the scattering angle and maximize the signal for the available satellite passes. The viewing geometry also impacts the ground sample distance, which is different for each observation. Supplementary Methods Table 2 shows the geometric mean of the ground sample distance for both camera axes. The C1 observation has the highest viewing zenith angle, and consequently, the largest ground sample distance. The uncertainty on the emission rate is obtained from the errors on the IME model, the retrieved CH_4 column density, and the wind speed, all added in quadrature. Wind speed error dominates the final error as it comes from a global meteorological model with coarse spatial resolution which can be inaccurate at the plume location.

The difference in emission rates between the C1 and C4 observations (~60 t/hr) are noteworthy given the equivalent changes in P-NAER$_{NS2A}$ emission rates are much smaller over the same period (~12 t/hr). Two possible reasons are identified for the larger than expected difference between C1 and C4 observations:

1. The larger scattering angle on C4 reduces the signal levels by a factor of about 25 compared to C1; and
2. The plume detected in the C1 observation consisted of a steady streamlined plume that spanned the length of the observation, whereas the plume detected in C4 had a dispersed morphology possibly owing to increased atmospheric turbulence or emission rate fluctuations.

To test whether the low signal levels or glint viewing geometry may have contributed to the low retrieved emission rate for C4 compared to C1, GHGSat conducted two controlled releases on land to simulate the Nord Stream viewing conditions of low signal and high viewing angle, separately. Test 1 comprised a high signal (albedo=0.6) and high viewing angle (70 degrees) observation. Test 2 comprised a low signal (albedo=0.06) and normal viewing angle (40 degrees) observation over snow. In both Tests, GHGSat retrieved source rates were within the uncertainty of the rates released on the ground, although a source rate which was on the low end of the uncertainty range was retrieved for Test 1. However, because both C1 and C4 had high viewing angles during the Nord Stream observations, this would not explain any discrepancy between the emission rates. Therefore, these tests did not reveal any clear explanation for the discrepancy between C1 and C4 relating to signal strength. This suggests that the increased atmospheric turbulence and emission rate fluctuations observed during C4 are the likely reason for the discrepancy. Although not verifiable, changing emission conditions during the final hours of leaking as the momentum of the ascending plume slowed may have caused these emission rate fluctuations at the sea surface.

Full Reference List – Harris et al.

1. Leaks in Nord Stream 1 and 2 will cause serious climate damage. *German Environment Agency* https://www.umweltbundesamt.de/en/press/pressinformation/leaks-in-nord-stream-1-2-will-cause-serious-climate (2022).
2. Sanderson, K. What do Nord Stream methane leaks mean for climate change? *Nature News* https://doi.org/10.1038/d41586-022-03111-x (2022).
3. Plejdrup, M.S. *Emission calculations for leaks on the Nord Stream 1 and 2 pipelines* [in Danish] (Aarhus University, DCE – National Center for Environment and Energy, 2023).
4. Gas-Lecks bei Nord Stream 1 & 2. *Leibniz Institute for Baltic Sea Research Warnemünde* https://www.io-warnemuende.de/im-fokus-details/items/gas-lecks-bei-nord-stream-1-2.html (2022).
5. The possible climate effect of the gas leaks from the Nord Stream 1 and Nord Stream 2 pipelines. *Danish Energy Agency* https://ens.dk/en/press/possible-climate-effect-gas-leaks-nord-stream-1-and-nord-stream-2-pipelines (2022).
6. Kouznetsov, R., et al. A bottom-up emission estimate for the 2022 Nord Stream gas leak: derivation, simulations, and evaluation. *Atmos. Chem. Phys*. **24**, 4675–4691 (2024).
7. Poursanidis, K., Sharanik, J. & Hadjistassou, C. World's largest natural gas leak from nord stream pipeline estimated at 478,000 tonnes. *iScience*. **27**, 108772 (2024).
8. Jia, M. et al. The Nord Stream pipeline gas leaks released approximately 220,000 tonnes of methane into the atmosphere. *Environ. Sci. & Ecotech.* **12**, 100210 (2022).
9. Mohrmann, M., Biddle, L.C., Rehder, G., Bittig, H. & Queste, B.Y. Nord Stream methane leaks spread across 14% of Baltic waters. *Nat. Commun*. (in the press).
10. Abrahamsson, K. et al. Methane plume detection after the 2022 Nord Stream pipeline explosion in the Blatic Sea. *Sci*. *Rep*. **14**, 12848 (2024).

11. Reum, F. et al. Diffusive methane emissions around the Nord Stream leak sites captured by airborne measurements. *Nat. Commun*. (in the press).

12. Dogniaux, M., Maasakkers, J.D., Varon, D.J. & Aben, I., Report on Landsat 8 and Sentinel-2B observations of the Nord Stream 2 pipeline methane leak. *Atmos. Meas. Tech*. **17**, 2777-2787 (2024).

13. MacLean, J-P. W., et al. Offshore methane detection and quantification from space using sun glint measurements with the GHGSat constellation. *Atmos. Meas. Tech*. **17**, 863-874 (2024).

14. Wilson, C., et al. Quantifying large methane emissions from the Nord Stream pipeline gas leak of September 2022 using IASI satellite observations and inverse modelling. *Atmos. Chem. Phys.* **24**, 10639–10653 (2024).

15. CAMS simulates methane emissions from Nord Stream pipelines leaks. *Copernicus Atmosphere Monitoring Service* https://atmosphere.copernicus.eu/cams-simulates-methane-emissions-nord-stream-pipelines-leaks (2022).

16. Orjollet S. Nord Stream leaked less methane than feared: atmospheric monitor. *Phys.org* https://phys.org/news/2022-10-nord-stream-leaked-methane-atmospheric.html (2022).

17. Ramonet, M., Berchet, A., Pison, I., & Ciais, P. Suivi du panache de méthane émis par les fuites des gazoducs Nord Stream en mer Baltique. *La Météorologie* **119**, 6–8 (2022).

18. Solbakken, C. F. Improved estimates of Nord Stream leaks. *NILU* https://www.nilu.com/2022/10/improved-estimates-of-nord-stream-leaks/ (2022).

19. Global Methane Pledge (UNEP CCAC, 2021); https://www.ccacoalition.org/resources/global-methane-pledge.

20. von Deimling, J. S., Linke, P., Schmidt, M., & Rehder, G. Ongoing methane discharge at well site 22/4b (North Sea) and discovery of a spiral vortex bubble plume motion. *Mar. Pet. Geol.* **68**, 718–730 (2015).

21. Rehder, G., Keir, R.S., Suess, E. & Pohlmann, T. The Multiple Sources and Patterns of Methane in North Sea Waters. *Aquat. Geochem.* **4**, 403–427 (1998).

22. Yvon-Lewis, S.A., Hu, L., & Kessler, J. Methane flux to the atmosphere from the Deepwater Horizon oil disaster. *Geophys. Res. Lett.* **38**, L01602 (2011).

23. Kessler, J.D. et al. A persistent oxygen anomaly reveals the fate of spilled methane in the deep Gulf of Mexico. *Science* **331**, 312–315 (2011).

24. Lee, J. D. et al. Flow rate and source reservoir identification from airborne chemical sampling of the uncontrolled Elgin platform gas release. *Atmos. Meas. Tech.* **11**, 1725–1739 (2018).

25. Operations. *Nord Stream AG* https://www.nord-stream.com/ (2023).

26. *Espoo Report Ch. 4 - Description of the Project* (Nord Stream AG, 2009); https://www.nord-stream.com/press-info/library/?per_page=100&q=&type=3&category=&country=.

27. *Background Information* (Nord Stream AG, 2016); https://www.nord-stream.com/download/document/10/?language=en.

28. *Navigational warning: The Baltic Sea* NW-230-22 (Danish Maritime Authority, 2022); https://nautiskinformation.soefartsstyrelsen.dk/details.pdf?messageId=72b2c3b1-0d0d-4a14-9ee0-be96c0a699fb&language=en.

29. GEUS has registered tremors in the Baltic Sea. *Geological Survey of Denmark and Greenland* https://www.geus.dk/om-geus/nyheder/nyhedsarkiv/2022/sep/seismologi (2022).

30. *European Marine Observation and Data Network (EMODnet): Bathymetry Data* (European Commission, 2023); https://emodnet.ec.europa.eu/en.

31. Botnariuc, L. et al. Investigating the Nord Stream Attack. *SPIEGEL International* https://www.spiegel.de/international/europe/investigating-the-attack-on-nord-stream-all-the-clues-point-toward-kyiv-a-124838c7-992a-4d0e-9894-942d4a665778 (2023).

32. *Navigational warning: The Baltic Sea* NW-235-22 (Danish Maritime Authority, 2022); https://nautiskinformation.soefartsstyrelsen.dk/details.pdf?messageId=8166360e-4f40-4b43-b2a1-4aa81f9f1552&language=en (2022).

33. Ringstrom, A. Gazprom lowers pressure in undamaged part of Nord Stream 2 pipe, Denmark says. *Reuters* https://www.reuters.com/business/energy/gazprom-lowers-pressure-undamaged-part-nord-stream-2-pipe-denmark-says-2022-10-05/ (2022).

34. *Erdgas - Orientierungswerte 2021* (Open Gas Europe, 2022); https://gitfront.io/r/StephenHarrisUNEPIMEO/Emq51iMoNq3M/Available-Data-for-Harris-et-al-Methane-emissions-from-the-Nord-Stream-subsea-pipeline-leaks/.

35. *Estimate of Total Methane Emissions from the Nord Stream Gas Leak Incident* Draft Working Paper (United Nations Environment Programme & International Methane Emissions Observatory, 2023); https://wedocs.unep.org/20.500.11822/41838.

36. Acton, M., Baldwin, P., Baldwin, T. & Jager, E. The development of the PIPESAFE risk assessment package for gas transmission pipelines. In *Proc. 1998 2nd International Pipeline Conference* 1–7 (ASME, 1998).

37. Préa, R. et al. CATHARE-3 V2.1: The new industrial version of the CATHARE code. In *ATH'20-Advances in Thermal Hydraulics 2020*. https://cea.hal.science/cea-04087378 (American Nuclear Society, 2020).

38. Danes: Nord Stream 2 pipeline seems to have stopped leaking. *Associated Press* https://apnews.com/article/russia-ukraine-putin-united-states-germany-business-afebd99d298ac72192acfeabfe384609 (2022).

39. Dissanayake, A.L., Gros, J., Drews, H.J., Nielsen, J.W. & Drews, A. Fate of Methane from the Nord Stream Pipeline Leaks. *Environ. Technol. Lett.* **10**, 903–908 (2023).

40. Schmale, O. et al. Distribution of methane in the water column of the Baltic Sea. *Geophys. Res. Lett* **37**, L12604 (2010).

41. Pätzold, F. et al. HELiPOD – revolution and evolution of a helicopter borne measurement system for multidisciplinary research in demanding environments. *Elem. Sci. Anth.* **11**, 00031 (2023).

42. Varon, D.J., et al. Quantifying Methane Point Sources from Fine-Scale Satellite Observations of Atmospheric Methane Plumes. *Atmos. Meas. Tech.* **11**, 5673–5686 (2018).

43. Varon, D.J. et al. High-frequency monitoring of anomalous CH_4 point sources with multispectral Sentinel-2 satellite observations. *Atmos. Meas. Tech.* **14**, 2771–2785 (2021).

44. ICOS RI, et al. ICOS Atmosphere Release 2023-1 of Level 2 Greenhouse Gas Mole Fractions of CO2, CH4, N2O, CO, meteorology and 14CO2, and flask samples analysed for CO2, CH4, N2O, CO, H2 and SF6. https://meta.icos-cp.eu/collections/hx5_JRH1Pgt_olBUkru5vxa5 (2023).

45. Conley, S. et al. Methane emissions from the 2015 Aliso Canyon blowout in Los Angeles, CA. *Science* **351**, 1317–1320 (2016).

46. *Global Methane Tracker 2023* (IEA, 2023); https://www.iea.org/reports/global-methane-tracker-2023.

47. Acton, M., Baldwin, T. & Jager, E. Recent developments in the design and application of the PIPESAFE risk assessment package for gas transmission pipelines. In *Proc. 2002 4th International Pipeline Conference* 831–839 (ASME, 2002).

48. Acton, M.R., Hankinson, G., Ashworth, B.P., Sanai, M. & Colton, J.D. A Full-Scale Experimental Study of Fires following the Rupture of Natural Gas Transmission

Pipelines. In *Proc. 2000 3rd International Pipeline Conference* V001T01A008 (ASME, 2000).

49. Acton, M., Dimitriadis, K., Potts, S. & Warhurst, K. Risk Assessment of Natural Gas Transmission Pipelines at Major River Crossings. *Hazards* **27**, 1–12 (2017).
50. Mauger, G., Tauveron, N., Bentivoglio, F. & Ruby, A. On the dynamic modeling of Brayton cycle power conversion systems with the CATHARE-3 code. *Energy* **168** (2019).
51. Barre, F. & Bernard, M. The CATHARE code strategy and assessment. *Nucl. Eng. Des.* **124**, 257–284 (1990).
52. Bestion, D. The physical closure laws in the CATHARE code. *Nucl. Eng. Des.* **124**, 229–245 (1990).
53. Tenchine, D. et al. Status of CATHARE code for sodium cooled fast reactors. *Nucl. Eng. Des.* **245**, 140–152 (2012).
54. Lemmon, E.W., Huber, M.L. & McLinden, M.O. NIST Standard Reference Database 23: reference fluid thermodynamic and transport properties-REFPROP. Version 8.0 (2013).
55. Kunz, O. & Wagner, W. The GERG-2008 wide-range equation of state for natural gases and other mixtures: an expansion of GERG-2004. *J. Chem. Eng. Data* **57**, 3032–3091 (2012).
56. Zigrang, D.J. & Sylvester, N.D. Explicit approximations to the solution of Colebrook's friction factor equation. *AICHE* **28**, 514–515 (1982).
57. Colburn, A.P. A method of correlating forced convection heat-transfer data and a comparison with fluid friction. *Int. J. Heat Mass Transf.* **7**, 1359–1384 (1964).

58. Siddans, R. et al. Global height-resolved methane retrievals from the Infrared Atmospheric Sounding Interferometer (IASI) on MetOp *Atmos. Meas. Tech.* **10**, 4135–4164 (2017).
59. Knappett, D., Siddans, R., Ventress, L., Kerridge, B. & Latter, B. STFC RAL methane retrievals from IASI on board MetOp-B,version 2.0, dataset. NERC EDS Centre for Environmental Data Analysis, https://catalogue.ceda.ac.uk/uuid/4bbcb1722f2842c1b0a5ebc19160a863/ (2022).
60. Wilson, C. et al. Contribution of regional sources to atmospheric methane over the Amazon Basin in 2010 and 2011. *Global Biogeochem. Cycles* **30**, 400–420 (2016).
61. Wilson, C. et al. Large and increasing methane emissions from eastern Amazonia derived from satellite data, 2010–2018. *Atmos. Chem. Phys.* **21**, 10643–10669 (2021).
62. Lund Myhre, C., Platt, S., Lunder, C. & Hermansen, O. ICOS ATC CH4 Release, Birkenes (75.0 m), 2020-09-14–2023-03-31, ICOS RI. *ICOS* https://hdl.handle.net/11676/0vifL2UB53ib1KiFVeWd63NS (2023).
63. Lehner, I. & Mölder, M. ICOS ATC CH4 Release, Norunda (58.0 m), 2017-04-01–2023-03-31, ICOS RI. *ICOS* https://hdl.handle.net/11676/mcZCu-5WouAxMyUJ8RJZ9y5j (2023).
64. Lund Myhre, C., Platt, S., Hermansen, O. & Lunder, C. ICOS ATC CH4 Release, Zeppelin (15.0 m), 2017-07-27–2023-03-31, ICOS RI. *ICOS* https://hdl.handle.net/11676/_SsoN8BWSu3N8-gSfq1Mfq9e (2023).
65. Pisso, I. et al. The Lagrangian particle dispersion model FLEXPART version 10.4. *Geosci. Model Dev.* **12**, 4955–4997 (2019).
66. Tarantola, A. *Inverse Problem Theory and Methods for Model Parameter Estimation.* Society for Industrial and Applied Mathematics. (2005).

67. Lehner, I. & Mölder, M. ICOS ATC CH4 Release, Norunda (100.0 m), 2017-04-01–2023-03-31, ICOS RI. *ICOS* https://hdl.handle.net/11676/QIUVe7wmfKcrMMO1yuXpae4c. (2023).

68. Heliasz, M. & Biermann, T. ICOS ATC CH4 Release, Hyltemossa (150.0 m), 2017-04-17–2023-03-31, ICOS RI. *ICOS* https://hdl.handle.net/11676/FNZRScPT_pVnFaZirluLEpFl (2023).

69. Hatakka, J. & Laurila, T. ICOS ATC CH4 Release, Utö - Baltic sea (57.0 m), 2018-03-09–2023-03-31, ICOS RI. *ICOS* https://hdl.handle.net/11676/fumW3pRc4v-JBVgu_ut72193 (2023).

70. Zängl, G., Reinert, D., Rípodas, P. & Baldauf, M. The ICON (ICOsahedral Non-hydrostatic) modelling framework of DWD and MPI-M: Description of the non-hydrostatic dynamical core. *Q. J. Roy. Meteorol. Soc.* **141**, 563–579 (2015).

71. Schröter, J. et al. ICON-ART 2.1: A flexible tracer framework and its application for composition studies in numerical weather forecasting and climate simulations. *Geosci. Model Dev.* **11**, 4043–4068 (2018).

72. Heliasz, M. & Biermann, T. ICOS ATC CH4 Release, Hyltemossa (70.0 m), 2017-04-17–2023-03-31, ICOS RI. *ICOS* https://hdl.handle.net/11676/FdKjV8DuFgh6jxrd7TSqqD2f (2023).

73. Lin, J. et al. A near-field tool for simulating the upstream influence of atmospheric observations: The Stochastic Time-Inverted Lagrangian Transport (STILT) model. *J. Geophys. Res. Atmos.* **108**, 4493 (2013).

74. Gerbig, C., Lin, J., Wofsy, S. Daube, B., Andrews, A., Stephens, B. Bakwin, P., and Grainger, C., Toward constraining regional-scale fluxes of CO2 with atmospheric observations over a continent: 2. Analysis of COBRA data using a receptor-oriented

framework, Journal of Geophysical Research-Atmospheres, 2003, 108, 4757, doi:10.1029/2003JD003770.

75. National Centers for Environmental Prediction/National Weather Service/NOAA/US Department of Commerce. NCEP GFS 0.25 degree global forecast grids historical archive. *Research Data Archive at the National Center for Atmospheric Research, Computational and Information Systems Laboratory* https://doi.org/10.5065/D65D8PWK (2015).

76. Lund Myhre, C., Platt, S., Lunder, C. & Hermansen, O. ICOS ATC CH4 Release, Birkenes (10.0 m), 2020-09-14–2023-03-31, ICOS RI. *ICOS* https://hdl.handle.net/11676/75hLzzO1hVvMUgJNb4z-OnXM, (2023).

77. Heliasz, M. & Biermann, T. ICOS ATC CH4 Release, Hyltemossa (30.0 m), 2017-04-17–2023-03-31, ICOS RI. *ICOS* https://hdl.handle.net/11676/Le3qzCL2U56Ya2gvI1ZHYlSR (2023).

78. Manders, et al. Curriculum vitae of the LOTOS–EUROS (v2.0) chemistry transport model. *Geosci. Model Dev.* **10**, 4145–4173 (2017).

79. Timmermans, R.D. Evaluation of modelled LOTOS-EUROS with observational based PM10 source attribution, *Atmos. Env.: X* **14**, 100173 (2022).

80. Kuenen, J. et al. CAMS-REG-v4: a state-of-the-art high-resolution European emission inventory for air quality modelling. *Earth Syst. Sci. Data* **14**, 491–515 (2022).

81. Agusti-Panareda, A., Diamantakis, M., Bayona, V., Klappenbach, F. & Butz, A. Improving the inter-hemispheric gradient of total column atmospheric CO2 and CH4 in simulations with the ECMWF semi-Lagrangian atmospheric global model. *Geosci. Model Dev.* **10**, 1–18 (2017).

82. Fortems-Cheiney, A. et al. Variational regional inverse modeling of reactive species emissions with PYVAR-CHIMERE-v2019. *Geosci. Model Dev.* **14**, 2939–2957 (2021).

83. Berchet, A. et al. The Community Inversion Framework v1.0: a unified system for atmospheric inversion studies. *Geosci. Model Dev.* **14**, 5331–5354 (2021).

84. Monforti Ferrario, F. et al. EDGAR v6.0 Greenhouse Gas Emissions. European Commission, Joint Research Centre (JRC), Dataset, PID: http://data.europa.eu/89h/97a67d67-c62e-4826-b873-9d972c4f670b (2021).

85. Raivonen, M. et al. HIMMELI v1. 0: HelsinkI Model of MEthane buiLd-up and emIssion for peatlands. *Geosci. Model Dev.* **10**, 4665–4691 (2017).

86. Etiope, G., Ciotoli, G., Schwietzke, S. & Schoell, M. Gridded maps of geological methane emissions and their isotopic signature. *Earth Syst. Sci. Data* **11**, 1–22 (2019).

87. Petrenko, V.V. et al. Minimal geological methane emissions during the Younger Dryas–Preboreal abrupt warming event. *Nature* **548**, 443–446 (2017).

88. Weber, T., Wiseman, N.A. & Kock, A. Global ocean methane emissions dominated by shallow coastal waters. *Nat. comms.* **10**, 4584 (2019).

89. CAMS255_2021SC1_D55.5.2.1-2023-Part CH4_Contribution to documentation of products and services as provided within the scope of this contract - 2023_v1 Official reference number service contract: 2021/CAMS2_55_CEA/SC1. https://atmosphere.copernicus.eu/sites/default/files/2024-01/CAMS255_2021SC1_D55.5.2.1-2023-PartCH4_Contribution_to_documentation_of_products_and_services__v1.pdf (2023).

90. Lawson, A. Nord Stream 2 pipeline pressure collapses mysteriously overnight. *The Guardian* https://www.theguardian.com/business/2022/sep/26/nord-stream-2-pipeline-pressure-collapses-mysteriously-overnight/ (2022).

91. Harby, K., Chiva, S. & Muñoz-Cobo, J.L. Modelling and experimental investigation of horizontal buoyant gas jets injected into stagnant uniform ambient liquid. *Int. J. Multiph. Flow* **93**, 33–47 (2017).

92. Lund Myhre, C., Platt, S. M., Lunder, C. & Hermansen, O. ICOS ATC NRT CH4 growing time series, Birkenes (10.0m), 2022-03-01–2022-10-16, ICOS RI, https://hdl.handle.net/11676/a-OqGFe7Aga6-k7CHen39EyQ, (2022).

93. Lund Myhre, C., Platt, S., Lunder, C. & Hermansen, O. ICOS ATC CH4 Release, Birkenes (50.0 m), 2020-09-14–2023-03-31, ICOS RI, https://hdl.handle.net/11676/lMSx28tDaMg1owQ5DHJOU___, (2023).

94. Lund Myhre, C., Platt, S. M., Lunder, C. & Hermansen, O. ICOS ATC NRT CH4 growing time series, Birkenes (50.0m), 2022-03-01–2022-10-16, ICOS RI, https://hdl.handle.net/11676/QhtU7Bpi3hW63r_P_YRETTsU, (2022).

95. Lund Myhre, C., Platt, S. M., Lunder, C. & Hermansen, O. ICOS ATC NRT CH4 growing time series, Birkenes (75.0m), 2022-03-01–2022-10-16, ICOS RI, https://hdl.handle.net/11676/M1WVYeDMy6UtPnSvF6KKmq_L, (2022).

96. Hatakka, J. & Laurila, T. ICOS ATC NRT CH4 growing time series, Utö-Baltic sea (57.0m), 2022-03-01–2022-10-16, ICOS RI, *ICOS* https://hdl.handle.net/11676/yFO_L2onDwckHg_2194ej4Mx, (2022).

97. Heliasz, M. & Biermann, T. ICOS ATC NRT CH growing time series, Hyltemossa (30.0 m), 2022-03-01–2022-10-16, ICOS RI. *ICOS* https://hdl.handle.net/11676/l9QSNSWCe3fqCzL0iTwLU8la (2022).

98. Heliasz, M. & Biermann, T. ICOS ATC NRT CH4 growing time series, Hyltemossa (30.0m), 2022-03-01–2022-10-16, ICOS RI, *ICOS* https://hdl.handle.net/11676/l9QSNSWCe3fqCzL0iTwLU8la, (2022).

99. Heliasz, M. & Biermann, T. ICOS ATC NRT CH4 growing time series, Hyltemossa (70.0m), 2022-03-01–2022-10-16, ICOS RI, *ICOS* https://hdl.handle.net/11676/lV2WF-vf84LsT73z6kWFJgV4, (2022).

100. Heliasz, M. & Biermann, T. ICOS ATC NRT CH4 growing time series, Hyltemossa (150.0m), 2022-03-01–2022-10-16, ICOS RI, *ICOS* https://hdl.handle.net/11676/-uYDRenkp8mfYPJLhekmx9Ko, (2022).

101. Lehner, I. & Mölder, M. ICOS ATC NRT CH4 growing time series, Norunda (32.0m), 2022-03-01–2022-10-16, ICOS RI, https://hdl.handle.net/11676/1hIMjlfGI_pDmu8CLT2DNB4R, (2022).

102. Lehner, I. & Mölder, M. ICOS ATC NRT CH4 growing time series, Norunda (58.0m), 2022-03-01–2022-10-16, ICOS RI, https://hdl.handle.net/11676/vZQwyfmtyDbICceVXxEefe7h, (2022).

103. Lehner, I. & Mölder, M. ICOS ATC CH4 Release, Norunda (100.0 m), 2017-04-01–2023-03-31, ICOS RI, https://hdl.handle.net/11676/QIUVe7wmfKcrMMO1yuXpae4c, (2023).

104. *Espoo Report: Nord Stream 2* W-PE-EIA-POF-REP-805-040100EN. *Rambøll A/S* https://prodstoragehoeringspo.blob.core.windows.net/3200e5b6-ac7d-4c43-8432-b5704f532947/Nord%20Stream%202,%20Espoo%20report%20-%20English.pdf (2017).

105. The first Nord Stream 2 string filled with technical gas. *Nord Stream 2* https://web.archive.org/web/20220120045759/https:/www.nord-stream2.com/media-info/news-events/the-first-nord-stream-2-string-filled-with-technical-gas-154/ (2021).

106. Second Nord Stream 2 String Filled with Technical Gas. *Nord Stream 2* https://web.archive.org/web/20220119203619/https:/www.nord-stream2.com/media-info/news-events/second-nord-stream-2-string-filled-with-technical-gas-156/ (2021).

107. *Espoo Atlas: Nord Stream 2* W-PE-EIA-POF-DWG-805-040100EN. *Rambøll A/S* https://ens.dk/sites/ens.dk/files/OlieGas/nord_stream_2_espoo_atlas_-_english_part_1.pdf (2017).

108. *Erdgas - Orientierungswerte 2022* (Open Gas Europe, 2023); https://oge.net/_Resources/Persistent/b/b/3/e/bb3e99d510987606aafbf73c09ea23f60c03248f/OGE%20Erdgas-Orientierungswerte%202022%20Stand%2021_03_2023.pdf.

109. Harby, K., Chiva, S. & Muñoz-Cobo, J.L. Modelling and experimental investigation of horizontal buoyant gas jets injected into stagnant uniform ambient liquid. *Int. J. Multiph. Flow* **93**, 33–47 (2017).

110. McVeigh, K. & Oltermann, P. Nord Stream gas leaks may be biggest ever, with warning of 'large climate risk'. *The Guardian* https://www.theguardian.com/environment/2022/sep/28/nord-stream-methane-gas-leaks-may-be-biggest-ever-with-warning-large-climate-risk (2022).

111. Ames, N. Nord Stream gas pipeline leaks threaten climate. *Energy Connects* https://www.energyconnects.com/opinion/features/2022/october/nord-stream-gas-pipeline-leaks-threaten-climate/ (2022).

112. Macnamara, K. Experts Estimate The Scale of The Nord Stream Pipelines Methane Leak. *Science Alert* https://www.sciencealert.com/experts-estimate-the-scale-of-the-nord-stream-pipelines-methane-leak (2022).

113. SILAM, System for Integrated modeLling of Atmospheric composition, https://silam.fmi.fi/ (2024).

114. SLB. https://www.slb.com/products-and-services/delivering-digital-at-scale/software/olga/olga-dynamic-multiphase-flow-simulator, (2024).

115. Socolofsky, S.A. et al. Texas A&M Oilspill Calculator (TAMOC): Modeling Suite for Subsea Spills. In: Proceedings from Arctic Marine Oil Pollution Technical Seminar on Environmental Contamination and Response. British Columbia, Canada, (2015).

116. Gros, J. et al. Petroleum dynamics in the sea and influence of subsea dispersant injection during Deepwater Horizon. *Proc. Nat. Acad. Sci.* **114**, 10065–10070 (2017).

117. 4th leak reported on Nord Stream pipelines. *Associated Press* https://www.youtube.com/watch?v=AsF7HhmfURE (2022).

118. Sloan Jr, E.D. & Koh, C.A. *Clathrate hydrates of natural gases*. CRC press. (2007).

119. Munkejord, S.T. et al. Depressurization of CO_2 in a pipe: High-resolution pressure and temperature data and comparison with model predictions. *Energy* **211**, 118560 (2020).

120. Hendricks, R.C., Simoneau, R.J. & Barrows, R.F. Two-phase choked flow of subcooled oxygen and nitrogen. NASA Technical Note D-8169, (1976).

121. Lanfredini, M. Critical flow prediction by system codes – Recent analyses made within the FONESYS network. *Nucl. Eng. Des.* **366**, 110731 (2020).

122. Hendricks, R.C. & Simoneau, R.J. Two phase choke flow in tubes with very large L/D. *Cryog. Eng. Conf.*, E-9279 (1977).

123. Jacobs, E. et al. Upwelling-induced trace gas dynamics in the Baltic Sea inferred from 8 years of autonomous measurements on a ship of opportunity. *Biogeosciences* **18**, 2679–2709 (2021).

124. Wiesenburg, D.A. & Guinasso Jr, N.L. Equilibrium solubilities of CH_4, carbon monoxide, and hydrogen in water and sea water. *J. Chem. Eng. Data* **24**, 356–360 (1979).

125. Aghito, M. et al. ChemicalDrift 1.0: an open-source Lagrangian chemical fate and transport model for organic aquatic pollutants. *Geosci. Model Dev.* **16**, 2477–2494 (2023).

126. Tuomi, L. et al. Overview of CMEMS BAL MFC Service and Developments. Proceedings of the Eight EuroGOOS International Conference, 3–5 (2017).

127. E.U Copernicus Marine Service Information (CMEMS). Baltic Sea Physics Reanalysis. *Marine Data Store (MDS)*. https://doi.org/ 10.48670/moi-00013. (2022).

128. Wanninkhof, R. Relationship between wind speed and gas exchange over the ocean revisited. *Limnol Oceanogr. Methods* **12**, 351–362 (2014).

129. Miller, S.M. et al. Observational constraints on the distribution, seasonality, and environmental predictors of North American boreal CH4 emissions. *Global Biogeochem. Cycles* 28, 146–160 (2014).

130. Sánchez-García, E., Gorroño, J., Irakulis-Loitxate, I., Varon, D. & Guanter, L. Mapping CH4 plumes at very high spatial resolution with the WorldView-3 satellite. *Atmos. Meas. Tech.* 15, 1657–1674 (2022).

131. Jervis, D. et al. The GHGSat-D Imaging Spectrometer. *Atmos. Meas. Tech.* 14, 2127–2140 (2021).